Phlogopite-Olivine Nephelinites Erupted During Early Stage Rifting, North Tanzanian Divergence

Céline Baudouin, Fleurice Parat

frontiers in Earth Science

ORIGINAL RESEARCH
published: 14 July 2020
doi: 10.3389/feart.2020.00277

Phlogopite-Olivine Nephelinites Erupted During Early Stage Rifting, North Tanzanian Divergence

Céline Baudouin[1] and Fleurice Parat[2]*

[1] *Centre de Recherches Pétrographiques et Géochimiques, UMR 7358 CNRS-UL, Vandœuvre-lés-Nancy, France,*
[2] *Géosciences Montpellier, UMR 5243 – CC 60 – Université de Montpellier, Montpellier, France*

The North Tanzanian Divergence (NTD, eastern branch of the East African Rift) corresponds to an early stage of continental breakup. In the southern NTD, two quaternary volcanoes of the Manyara-Balangida rift (Labait, Kwaraha) have erupted primary nephelinite lavas (Mg# = 79–57) that allow characterization of their deep mantle source and the alkaline magmas that percolated through the lithosphere during rift initiation. Nephelinites are olivine- and clinopyroxene-rich, and contain up to 4 vol% magmatic phlogopite that crystallized as a liquidus phase with olivine and clinopyroxene. The presence of hydrous mineral (phlogopite) phenocrysts in Kwaraha and Labait lavas strongly suggests that the alkaline melts were H_2O-bearing at the time of phlogopite crystallization (1.57–2.12 wt% H_2O in phlogopite), demonstrating that phlogopite may have influenced the partitioning of water between the silicate melt and anhydrous silicate minerals (<1 ppm wt H_2O clinopyroxene, 1–6 ppm wt H_2O in olivine). Geochemical modeling indicates that the nephelinite magmas resulted from a low degree of partial melting (0.2–1%) of a carbonate-rich (0.3%) garnet peridotite containing ∼2 vol% phlogopite. We estimate the depth of partial melting based on primary melt compositions and empirical relations, and suggest that melting occurred at depths of 110–130 km (4 GPa) for craton-edge lavas (Kwaraha volcano) and 150 km (5 GPa) for on-craton lavas (Labait volcano), close to or below the lithosphere-asthenosphere boundary in agreement with the presence of deep refractory mantle xenoliths in Labait lavas. The depth of melting becomes gradually deeper toward the southern NTD: highly alkaline magmas in the north (Engaruka-Natron Basin) are sourced from amphibole- and CO_2-rich peridotite at 75–90 km depth, whereas magmatism in the south (south Manyara Basin) is sourced from deep phlogopite- and CO_2-rich garnet-peridotite beneath the Tanzania craton (e.g., at the on-craton Labait volcano). Percolation of deep asthenospheric CO_2-rich alkaline magmas during their ascent may have produced strong heterogeneities in the thick sub-continental lithospheric mantle by inducing metasomatism and phlogopite crystallization in glimmerite lithologies.

Keywords: nephelinites, rift, partial melting, alkaline magmatism, metasomatism

OPEN ACCESS

Edited by:
Anastassia Borisova,
Centre National de la Recherche Scientifique (CNRS), France

Reviewed by:
Marlina A. Elburg,
University of Johannesburg, South Africa
Stephen Foley,
Macquarie University, Australia

****Correspondence:***
Céline Baudouin
baudouin.geol@gmail.com

Specialty section:
This article was submitted to Petrology, a section of the journal Frontiers in Earth Science

Received: *26 March 2020*
Accepted: *17 June 2020*
Published: *14 July 2020*

Citation:
Baudouin C and Parat F (2020) Phlogopite-Olivine Nephelinites Erupted During Early Stage Rifting, North Tanzanian Divergence. Front. Earth Sci. 8:277. doi: 10.3389/feart.2020.00277

INTRODUCTION

Silica-undersaturated magmas are abundant in continental rifts, including highly alkaline lavas such as melilitite, nephelinite, basanite, and phonolite. Low-silica lavas are commonly CO_2-rich and have been described as the product of CO_2-bearing mantle domains (e.g., Brey, 1978; Dasgupta et al., 2007) associated with carbonatite, suggesting a cogenetic origin (Woolley and Kjarsgaard, 2008). The oldest volcanism of the East African Rift (EAR, ∼45 Ma) occurred in Ethiopia associated with the propagation of the EAR toward the south (Ebinger et al., 2000) and produced abundant highly alkaline rocks and carbonatites (e.g., Pouclet et al., 1981; Foley et al., 2012). Melilitites and nephelinites were erupted at the tip of the propagating rift and around the Tanzanian craton (i.e., Tanzania, Uganda; Foley et al., 2012). In northern Tanzania, primitive lavas, erupted generally in monogenetic volcanic fields (e.g., the Engaruka-Natron monogenetic field), are characterized by small eruptive volumes, little fractional crystallization during ascent, relatively high ascent rates, and xenolith-bearing lavas (Mattsson et al., 2013).

Primary alkaline lavas erupted on and at the edge of the Tanzanian craton sampled mantle xenoliths that indicate the presence of heterogeneous sub-cratonic lithospheric and asthenospheric mantle domains related to metasomatism by carbonated (Jones et al., 1983; Rudnick et al., 1993; Lee and Rudnick, 1999; Foley et al., 2012) and/or H_2O-rich fluids (Dawson and Smith, 1988; Koornneef et al., 2009). The xenolith data suggest that primary lavas originate from deep asthenospheric mantle processes. Furthermore, alkaline lavas are volatile-rich (e.g., Ivanikov et al., 1998; Keller et al., 2006; Métrich and Wallace, 2008; Hudgins et al., 2015) and could only derive from deep, low-degree partial melting of H_2O-CO_2-bearing peridotites. The depth of origin, degree of partial melting, and mantle source control the alkalinity of the primary melt (e.g., Maaløe et al., 1992; Rogers et al., 1992). The diversity of alkaline lavas (melilitite, nephelinite, and basanite) erupted in the North Tanzanian Divergence (NTD) clearly indicates partial melting at various levels in the sub-cratonic lithosphere and asthenosphere (e.g., Rosenthal et al., 2009; Foley et al., 2012; Mana et al., 2015). Further differentiation by fractional crystallization, liquid immiscibility, and assimilation produced Mg-rich nephelinite, Mg-poor nephelinite, and carbonatite at different levels in the mantle and continental crust during ascent (Klaudius and Keller, 2006; Zaitsev et al., 2012; Baudouin et al., 2016).

In this paper, we performed a petrological and geochemical investigation of the most primitive lavas of the NTD, i.e., nephelinites from the Manyara basin (Kwaraha and Labait volcanoes) to determine the mantle conditions of silica-undersaturated magma genesis at the first stage of continental break-up. We discuss the presence of magmatic phlogopite in terms of alkaline magma composition and crystallization environment of these magmas, and model the partial melting of a deep metasomatized mantle source of the highly alkaline magmas beneath the eastern part of the Tanzanian Craton.

Geological Background

The EAR is divided into two branches which correspond to different stages of plate boundary extension, from rift initiation (eastern branch initiation: Manyara-Balangida basin, Tanzania, and western branch initiation: Toro-Ankole basin, Uganda) to oceanic stage in the Afar Triple Junction. In the eastern branch, volcanism began 30 Ma in northern Kenya, 15 Ma in central Kenya, and 6 Ma in northern Tanzania (Mana et al., 2012, 2015). The north Tanzanian rift splays to form the NTD, which includes large volcanic complexes (e.g., Ngorongoro, Meru, and Kilimanjaro) and small volcanic cones (e.g., Lashaine, Olmani) (Dawson et al., 1970, 1997; Jones et al., 1983). The southern NTD is divided into three rift areas: Eyasi, Manyara-Balangida, and Pangani, from west to east (Le Gall et al., 2008; **Figure 1**). The Eyasi and Pangani fault systems are amagmatic and represent rift propagation from the Natron basin to the western and eastern parts of the NTD, respectively. The Manyara-Balangida basin, representing southward rift propagation, lies along the rift escarpment and includes two volcanic centers (Hanang and Kwaraha volcanoes, **Supplementary Figures A1, A2**) surrounded by small volcanic cones (Labait and Sora Hill, respectively, Dawson, 2008). East of the Manyara basin, several volcanic centers have erupted relatively evolved nephelinite lavas, whereas small volcanic cones in the Monduli-Meru area have erupted primitive lavas. The most primitive lavas were erupted at Kwaraha and the small cones around Hanang and Meru. We sampled Labait and Kwaraha for this study (**Figure 1**).

Labait volcano (4°34′12″ S, 35°26′04″ E, near Hanang volcano) is a small olivine melilitite cone (Dawson et al., 1997; **Figure 1**). Eruptions at Labait occurred at 0.4 ± 0.2 Ma (Rudnick et al., 1999). Labait lavas carried abundant mantle xenoliths including spinel phlogopite harzburgites, garnet lherzolite-harzburgites, dunites, and glimmerite xenoliths (Lee and Rudnick, 1999; Koornneef et al., 2009). The presence of phlogopite-bearing xenoliths (lherzolite and glimmerite) strongly suggests the presence of H_2O-rich fluids within the lithosphere. Models of water diffusion profiles in mantle olivines indicate high ascent rates (4–28 $m{\cdot}s^{-1}$) and a low lithospheric mantle water content (<50 ppm wt H_2O) (Hui et al., 2015). Isotopic data from Labait olivine nephelinites indicate that cratonic or craton-margin lithosphere is present beneath Labait, with a slightly different signature compared to the lithospheric mantle (MacDonald et al., 2001; Aulbach et al., 2008).

Kwaraha volcano (4°13′45″ S, 35°48′53″ E) consists of Quaternary (1.5–0.7 Ma; Dawson, 2008) Mg-rich nephelinite agglomerates, tuffs, and lavas (Dawson et al., 1997). Tuff cones, craters, and a calciocarbonatite lava flow are distributed around the main edifice. Kwaraha lavas are derived from a source with similar isotopic ratio than the Proterozoic Mozambique mobile belt (low $^{87}Sr/^{86}Sr$; Paslick et al., 1996; MacDonald et al., 2001). Small parasitic cones produced lavas with melilitite to nephelinite compositions (Dawson et al., 1997) that are more mafic than those of the main edifice, and may represent the parental melt (Dawson et al., 1997; Dawson, 2008). We studied 10 parasitic cones including Sora Hill (Kw2) and Haindadonga cones (Kw3) (Dawson et al., 1997; **Figure 1**).

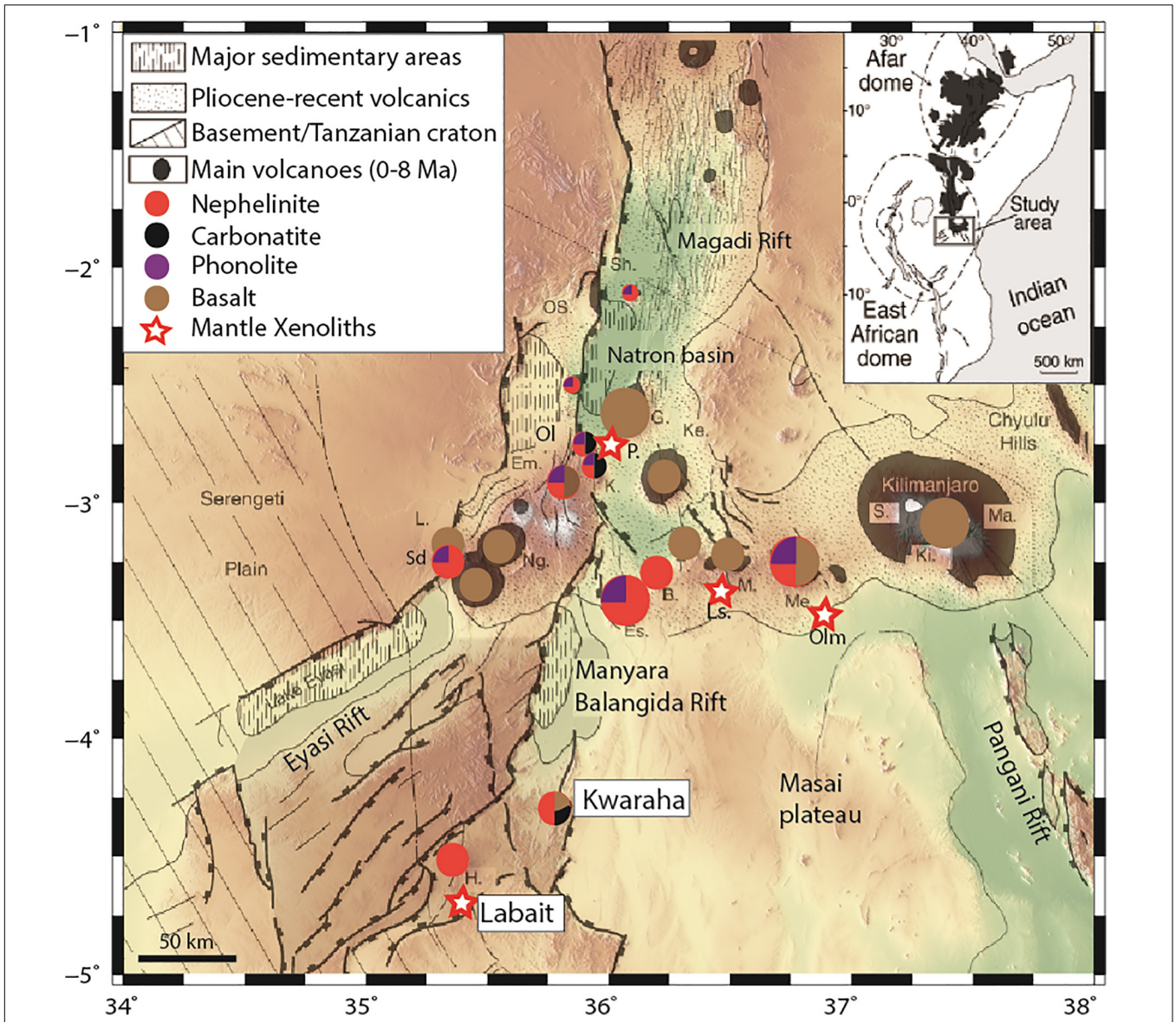

FIGURE 1 | Main structural and magmatic features of the North Tanzanian Divergence, and the locations of Labait and Kwaraha. Proportions of symbol colors represent relative eruptive volumes of magma composition for single volcano (nephelinite, phonolite, carbonatite, basalt). Volcano names are abbreviated as: B., Burko; Em., Embagai; Es., Essimingor; G., Gelai; H., Hanang; K., Kerimasi; Ke., Ketumbeine; Ki., Kibo; L., Lemagrut; M., Monduli; Ma., Mawenzi; Me., Meru; Ng., Ngorongoro; Ol., Oldoinyo Lengai; OS., Ol Donyo Sambu; P., Pello Hill; Sd., Sadiman; S., Shira; Sh., Shombole; T., Tarosero. Map modified after Le Gall et al. (2008).

MATERIALS AND METHODS

Major and Volatile Element Analyses

Whole-rock major element compositions were measured by inductively coupled plasma optical emission spectroscopy (iCap 6500 Thermo Fisher) at the Service d'Analyse des Roches et des Minéraux (SARM) at the Centre de Recherches Pétrographiques et Géochimiques (Nancy, France) following the protocol established by Carignan et al. (2001). One gram of whole-rock powder was dissolved with HNO_3 and the mixture (with $LiBO_2$) was fused. The reference standard was SLRS-5 and errors are estimated to be <2% (1σ).

Complementary whole-rock analyses has been performed by wide-angle X-ray fluorescence using sequential spectrometer Bruker S4 Pioneer at the analytical services of the Instituto Andaluz de Ciencias de la Tierra (IACT, University of Granada, Spain) using Rh X-ray tube (160 kV, 159 mA). Rock powders (1 g) are weighed with di-lithium tetraborate flux, and then the mixture is fused at 1000°C for 15 min. The concentrations of major elements in the samples are measured by comparing the X-ray intensity for each element with nine reference geological standard samples. Whole-rock sulfur and carbon contents were determined for each sample via elemental analyser, F and Cl contents were determined by wet precipitation-ferrithiocyanate

spectrophotometry using a Varian Cary 50 spectrophotometer. High LOI (up to 8 wt%), and CO_2 content (up to 4.6 wt%) in nephelinitic lavas are due to the presence of small size secondary minerals within the groundmass from hydrothermal alteration (i.e., calcite, zeolite). Such minerals are common in nephelinites as reported at Mount Etinde (Cameroon; Etame et al., 2012), Engaruka volcanic field (Neukirchen et al., 2010), Cape Verde (Mourão et al., 2012), and as well worldwide nephelinites and melilitites (Georoc database[1]; **Supplementary Table A1**).

Mineral major and volatile element concentrations were determined via electron microprobe (Cameca XS100 at Geoscience Montpellier, France). Analyses were performed with an accelerating voltage of 20 keV, a 10 nA beam current, and a focused (1 μm) beam. The counting time was fixed at 20 and 40 s for major and volatile element (S, Cl) analyses, respectively. The standards used for major and volatile element analyses were wollastonite for Si and Ca, Al_2O_3 for Al, TiO_2 for Ti, forsterite for Mg, hematite for Fe, orthoclase for K, albite for Na, apatite for P, native metal for Ni, Mn, and Cu, barite for S and Ba, fluorite for F, and chlorapatite for Cl.

Trace Element Analyses

Whole-rock trace element analyses of lavas from Kwaraha and related small volcanic cones (samples Kw1–Kw8), and Labait were performed by ICP mass spectrometry (ICP-MS) after HNO_3 and HF digestion of 0.1 g of sample powder in a Teflon-lined vessel at 180°C and 200 psi for 30 min, evaporation to dryness, and subsequent dissolution in 100 mL of 4 vol% HNO_3. Triplicate measurements were performed with a NexION 300d (Perkin Elmer) ICP-MS at the Instituto Andaluz de Ciencias de la Tierra (University of Grenada) using Rh as an internal standard, and using multi-element calibration solutions for external calibration. Analytical precision was better than ± 5% for concentrations > 10 ppm. Whole-rock analyses of samples Kw10, Kw11, and Kw12 were performed using a quadrupole 7700x ICP-MS at the Analyse des Eléments en Trace dans l'Environnement (AETE platform, OSU-OREME, University of Montpellier) where 0.1 g of whole-rock powder was dissolved with acid (HF-HNO_3). Blanks spiked with In and Bi were prepared to monitor instrumental drift. Solutions were analyzed at a final dilution factor of 4000. The sensitivity of the ICP-MS in this configuration was 200×10^6 /ppm ^{115}In. Analytical accuracy was estimated from measurements of international rock standards UBN and BEN for both analytical procedures (**Supplementary Table A1**).

Mineral trace element concentrations were determined by laser ablation ICP-MS at AETE using a GeoLas Q+ Excimer CompEx 102. A 26 and 56 μm diameter laser beam was used for apatite and silicate minerals, respectively, with a laser repetition rate of 6–10 Hz and laser power of 0.5 mJ (5 J·cm^{-2}). The spot size was chosen as a compromise between signal intensity and the size of the minerals of interest in the samples. Concentrations were calibrated with glass standard NIST612 and SiO_2 and CaO concentrations previously determined by electron microprobe. The BIR-1 standard was used as an external standard. Glitter Software (Griffin et al., 2008) was used to process the raw data files (signal intensity vs. time) into elemental concentrations. This allows precise selection of blanks and signals, and rapid visualization of the intensity data. Instrumental drift was compensated by internal standard calculations using Glitter; no other drift corrections were performed.

Water Content Analyses

The water contents of clinopyroxene and olivine (ol) were determined using Fourier transform infrared (FTIR) spectroscopy. Handpicked minerals were prepared as doubly polished sections with thicknesses between 140 and 325 μm. The hydrogen concentration was measured in transmission mode at the Laboratory Charles Coulomb (University of Montpellier, France). For olivine crystals, FTIR analyses were performed in the center of crystals far from iddingsite rims. Unpolarized infrared spectra were acquired using a Bruker IFS 66v coupled with a Hyperion optical microscope. A Globar light source and a Ge-KBr beam splitter were used to generate unpolarized mid-infrared radiation (4000–400 cm^{-1}). Water contents were calculated by integration of spectra between 3770 and 3000 cm^{-1} for clinopyroxene and between 3610 and 3000 cm^{-1} for olivine (for the detailed analytical method, see Denis et al., 2015). Water concentrations were calculated using the calibration of Paterson (1982), considering the water concentration as a function of the density of clinopyroxene ($\chi_{clinopyroxene}$(Kw3) = 2707 ppm wt H_2O, $\chi_{clinopyroxene}$(Kw5) = 2737 ppm wt H_2O) and olivine (χ_{ol}(Kw) = 2605–2612 ppm wt H_2O, χ_{ol}(Lab) = 2587 ppm wt H_2O). Errors on water contents due to the calibration (Paterson, 1982) and uncertainties on the sample thickness and background correction are ± 15% (Denis et al., 2015). The integrated unpolarized absorbances normalized to 1 cm sample thickness are also reported to use alternative mineral-specific FTIR calibrations.

The water content of phlogopite from sample Kw3 was measured on mineral separates by Karl-Fischer titration (KFT) using air as the transporting gas and muscovite as a standard (σ = 0.1 wt% H_2O) at the University of Hannover (Behrens et al., 1996). Whole rock H_2O content were measured by Karl Fischer titration at SARM. Standard solutions were used to check the accuracy of spectrophotometry analyses, and standard deviations are less than 5%.

RESULTS

All samples from Kwaraha (lava flows) and Labait (scoria) have microlitic porphyric textures with large phenocrysts of olivine and clinopyroxene (>1 mm) (**Figure 2**). Following the nomenclature of Le Bas (1989), the bulk rock compositions of Kwaraha lavas and Labait scoria are foidites with compositions between melilitite and nephelinite, similar to nephelinites reported in north Tanzania (**Figure 3**; Dawson et al., 1970, 1997; Mana et al., 2012). Because of the similar mineral assemblages and chemical compositions of all samples, as well the absence of melilite minerals, we refer to them herein as nephelinites.

[1] http://georoc.mpch-mainz.gwdg.de/georoc/

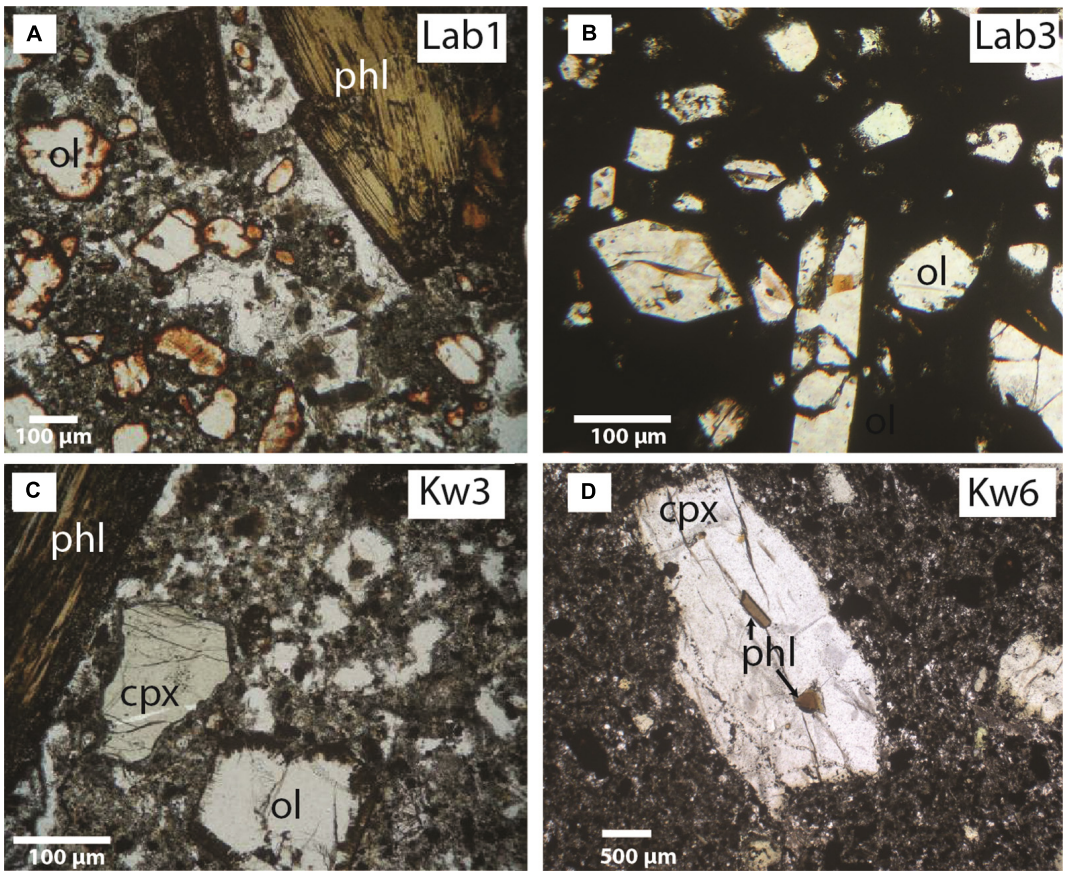

FIGURE 2 | Representative microphotographs of sampled lavas: nephelinites from **(A,B)** Labait (Lab1, Lab3), **(C,D)** Kwaraha (Kw3, Kw6) Abbreviations: ol, olivine; phl, phlogopite; clinopyroxene, cpx.

Labait Volcano

Petrography and Mineral Chemistry

Nephelinites from Labait volcano have microlitic textures with olivine phenocrysts (15–30 vol%, 0.5–4 mm) set in a groundmass of clinopyroxene, magnetite (magnesioferrite, Ti-magnetite) (<1 vol%), and pyrrhotite. Olivine rims are often transformed into iddingsite. Rare phlogopite phenocrysts (0.5–1 vol%, ∼1 mm) are present in samples Lab1 (**Figure 2**) and Lab2. Olivines have high forsterite (Fo) and NiO contents in Lab1 (Fo_{91} to Fo_{81}, 0.37–0.18 wt% NiO) and Lab3 (Fo_{89} to Fo_{87}, 0.45–0.24 wt% NiO) lavas (**Supplementary Figures A3, A4** and **Table 2**). Phenocrysts are normally zoned with decreasing MgO and NiO contents (Fo_{91} to Fo_{85}) and increasing CaO contents (0.04–0.61 wt%) from core to rim. One olivine from Lab1 with the lowest Fo content has reverse zoning with increasing Fo content toward the rim (Fo_{83} to Fo_{88}). The water content in olivine (Lab1) ranges from 2.5 to 6.6 ppm wt H_2O (**Figure 5** and **Table 4**).

Small clinopyroxene crystals (<30 mm) are present in the groundmass and have diopsidic compositions ($En_{40}Wo_{49}Fs_{11}$) with relatively low Mg# (78–79) (**Supplementary Figure A5**), high TiO_2 contents (2.5–3 wt%), low Na_2O (0.7–0.9 wt%) and Al_2O_3 contents (1.4–2 wt%), and very low Cr_2O_3 contents (<0.01 wt%).

Phlogopite phenocrysts (Mg# = 83–86) have relatively low F (0.2–0.8 ± 0.2 wt%), TiO_2 (3.6–3.7 wt%) and Al_2O_3 contents (12.2–12.4 wt%) (**Figure 6**). Trace element concentrations are 0.1–2.9 ppm La, 841–9359 ppm Ba, 97–267 ppm Rb, and 32–1395 ppm Sr (**Table 3** and **Figure 7**), and normalized trace element patterns display positive Zr-Hf anomalies.

Nepheline is present in the groundmass as Fe-rich microcrystals (10–20 µm, 2.3–3.4 wt% FeO). Labait lavas contain oxide phases including magnetite (7.3–8.6 wt% TiO_2, 0.8–1.2 wt% MgO), Cr-magnetite (30–50 wt% Cr_2O_3, 3.5–7.5 wt% TiO_2), Mg-magnetite (8.9–9.4 wt% TiO_2, 15–17.4 wt% MgO), and perovskite (55.2 wt% TiO_2) (**Supplementary Table A1** and **Supplementary Figure A6**). Rare apatite crystals are fluorapatites (3–4 wt% F) with low Cl (<0.02 wt%) and SO_3 contents (0.02–0.09 wt%). Sulfides are Ni-rich pyrrhotites (5.7 wt% Ni, 0.06 wt% Cu, 37.6–38.8 wt% S, Pd/Ir = 2–41) with chalcopyrite rims (0.2 wt% Ni, 31.5 wt% Cu, 34.7 wt% S) (**Supplementary Table A1**).

Whole Rock Geochemistry

Nephelinites have very high Mg# ($[Mg/(Mg + Fe_{tot})] \times 100$) values ranging from 76.5 to 79.3 (MgO = 24.8–28.3 wt%), variable peralkaline indices (Na + K/Al = 0.7–1.2) and K_2O/Na_2O ratios

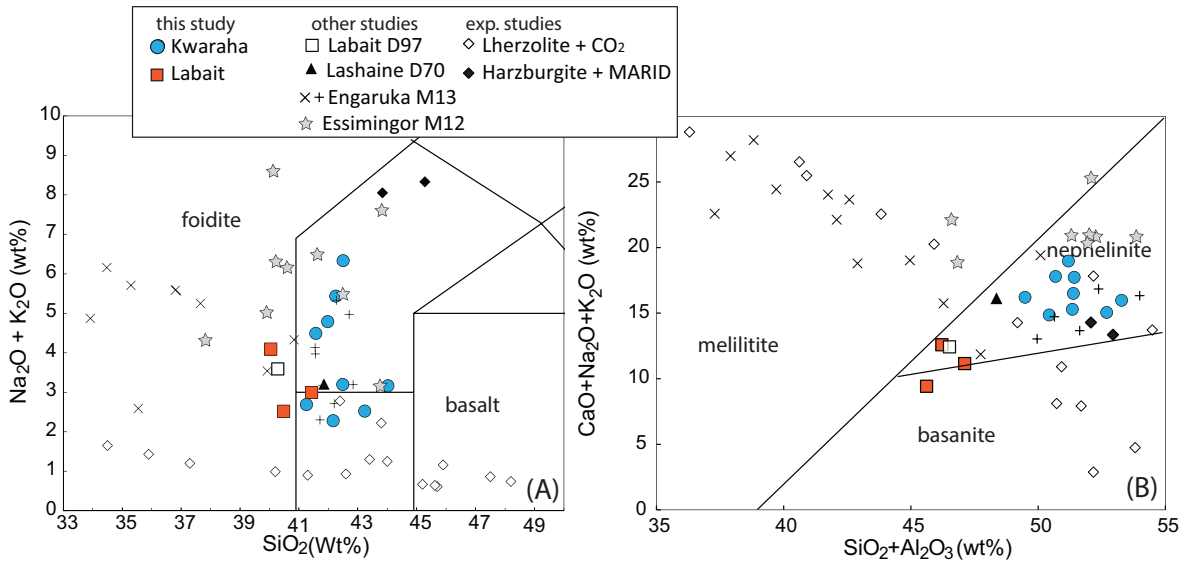

FIGURE 3 | Geochemical classification of sampled lavas from Kwaraha (circles) and Labait (squares). **(A)** Alkali vs. silica composition **(B)** melilitite-nephelinite-basanite classification (Le Bas, 1989). Whole rock data are recalculated anhydrous to 100%. We also reported literature data from Labait and Lashaine (triangle) lavas (Dawson et al., 1970, 1997, respectively), Essimingor lavas (gray stars; Mana et al., 2012), melilitites (plus) and nephelinites (cross) from Engaruka volcanic field (Mattsson et al., 2013). Experimental melt compositions from partial melting of lherzolite + CO_2 (open diamonds; Dasgupta et al., 2007) and Harzburgite + MARID (black squares; Förster et al., 2018) are also reported.

(0.7–1.1), low CaO contents (5–7.4 wt%), and moderate Al_2O_3 contents (5.4–6.1 wt%) (**Figure 4** and **Table 1**). Lavas have variable whole-rock volatile concentrations: 0.7–4.6 wt% CO_2, 2.12–2.54 wt% H_2O, 200–360 ppm S, 1100–1700 ppm F, and 44–71 ppm Cl. No correlations are observed amongst the volatiles. The high CO_2 content of Lab1 and Lab2 samples is related the occurrence of calcite in cracks, whereas no calcite or secondary phases within the groundmass has been observed in Lab3 nephelinitic sample (0.7 wt% CO_2). This sample (Lab3) is considered as fresh sample and whole rock data will be favored for models.

Labait lavas have high incompatible element concentrations up to 300 times chondritic rare earth element (REE) values with a high fractionation of light REEs (LREEs) compared to heavy REEs (HREEs) (La/Sm = 8.2–8.8, La/Yb = 69.1–71.7) (**Figure 8** and **Table 1**). Lavas have high large ion lithophile element (LILE) concentrations (e.g., 551–621 ppm Ba), and relatively low high field strength element (HFSE) contents (e.g., 168–178 ppm Zr) (**Figure 8**). Trace element patterns have negative K and Zr-Hf anomalies (**Figure 5**), high Zr/Hf (42.6–46), Ce/Y (8.4–8.7), Nb/U (52.2–53.9), and Rb/Sr ratios (0.05–0.08), and low Zr/Nb (2–2.3) and Ba/Rb ratios (8.5–13.3). Labait lavas are characterized by high Cr (495–1126 ppm) and Ni contents (827–1000 ppm).

Phlogopite-Bearing Xenoliths

Mantle xenoliths from Labait volcano have been studied previously by Rudnick et al. (1993) and Koornneef et al. (2009). We report here additional geochemical data for phlogopite-bearing mantle xenoliths: phlogopite-bearing lherzolites and glimmerites.

Phlogopite-bearing lherzolites (i.e., Labx6, **Table 2**) have porphyroclastic textures with 71–93 vol% olivine (Fo_{85} to Fo_{93}), 1–10 vol% clinopyroxene, (Mg# = 78–91), 11–24 vol% orthopyroxene (Mg# = 86–91), and 1–2 vol% Cr spinel [Cr# = 82–94; Cr# = Cr/(Cr+Al)] (Koornneef et al., 2009; Hui et al., 2015). Phlogopites occur as phenocrysts (0.1–1 mm), either disseminated throughout the sample or associated with spinel. They have high Mg# (90–92.6) and relatively high Al_2O_3 (14.6–15.8 wt%), TiO_2 (3.5–6.4 wt%), and Cr_2O_3 contents (0.17–1.86 wt%) (**Table 2** and **Figure 6**). Phlogopites have relatively low F (0.3–1.2 wt%) and very low Cl contents (<0.04 wt%). They have low REE (0.02–0.2 ppm La, <0.01 ppm Yb) and high LILE concentrations (1267–4310 ppm Ba, 178–274 ppm Rb, 30–33 ppm Sr) (**Table 3** and **Figure 7**).

Glimmerites (Labx7) contain 99 vol% phlogopite (<1% oxides). Phlogopites have low Mg# (83.7–84) and relatively low Al_2O_3 (12.9–13.2 wt%) and Cr_2O_3 contents (0.51–0.57 wt%) (**Table 2** and **Figure 6**). Phlogopites have low F (0.2–0.8 ± 0.2 wt%) and very low Cl contents (<0.03 wt%). They have low Ba (842–934 ppm), very low REE (<0.02 ppm La), and high Rb concentrations (323–358 ppm Rb) (**Table 3**).

Kwaraha Volcano

Petrography and Mineral Chemistry

Lavas sampled from small volcanic cones around Kwaraha volcano are nephelinites (n = 9, **Figure 3**) and one carbonatite (Kw1) was sampled from the main volcanic center. The nephelinites have microlitic textures and contain phenocrysts of

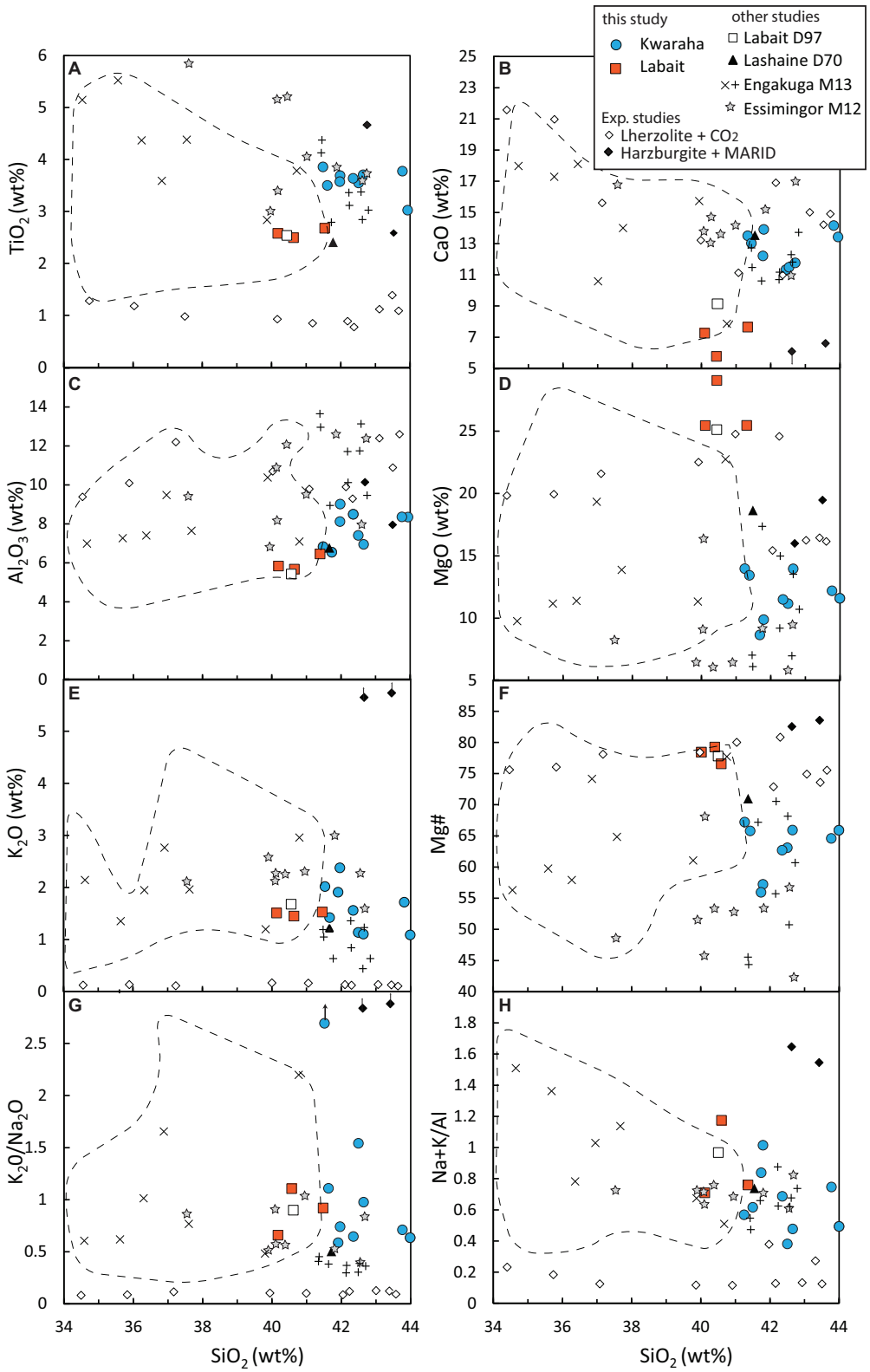

FIGURE 4 | Major element variation diagrams of sampled lavas from Kwaraha and Labait **(A)** TiO_2, **(B)** CaO, **(C)** Al_2O_3, **(D)** MgO, **(E)** K_2O, **(F)** Mg#, **(G)** K_2O/Na_2O, and **(H)** Na + K/Al vs. SiO_2 content. Continental melilitite compositions (dashed line) are from the Georoc database (http://georoc.mpch-mainz.gwdg.de/georoc/). All other symbols are as in **Figure 3**.

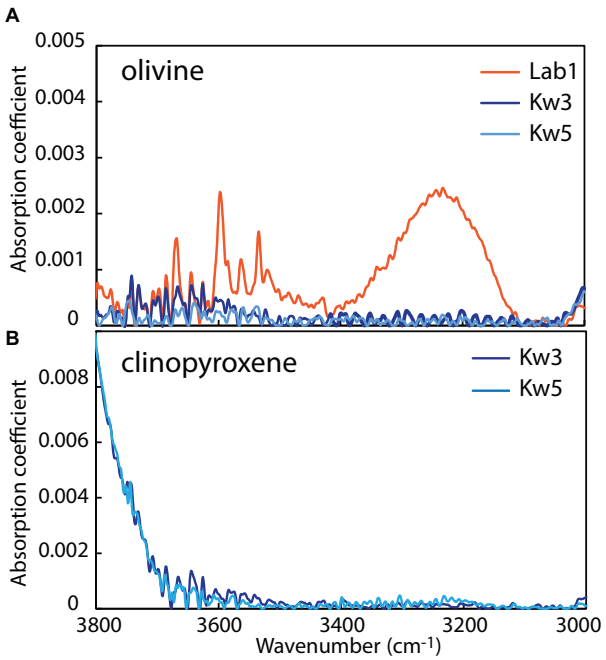

FIGURE 5 | Representative FTIR spectra of unoriented **(A)** olivine (4 ppm H_2O for Lab1 and < 1 ppm H_2O for Kw3, Kw5) and **(B)** clinopyroxene (<1 ppm H_2O for Kw3, Kw5) from Labait and Kwaraha lavas. All spectra are normalized to 1 cm thickness.

olivine (2–13 vol%, 0.2–7 mm), clinopyroxene (4–12 vol%, 0.2–8 mm), phlogopite (0–4 vol%, 0.2–10 mm), and magnetite (1–5 vol%, 0.5 mm) (**Figure 2**). Olivine, clinopyroxene, nepheline, and rare apatite occur as microcrystals in the groundmass.

Olivines from Kwaraha lavas have high Fo (Fo_{86} to Fo_{81}) and NiO contents (0.23–0.04 wt%) (**Supplementary Figure A4**). Olivine phenocrysts are normally zoned with decreasing MgO and NiO contents (Fo_{86} to Fo_{82} and 0.2–0.05 wt%, respectively) and increasing CaO contents from core to rim (0.17–0.83 wt%). Olivine water contents are very low, <2 ppm wt H_2O (**Table 4**).

Clinopyroxene phenocrysts have diopsidic compositions ($En_{35-48}Wo_{47-52}Fs_{2-16}$) with high Mg# (90–77), although rare clinopyroxene have low Mg# (63–74). High-Mg# clinopyroxene phenocrysts have 16.4–13.4 wt% MgO, 3.5–0.3 wt% Al_2O_3 (Al^{VI}/Al^{IV} = 0.89–0.56), and up to 1.1 wt% Cr_2O_3 (**Supplementary Figure A5**). REE patterns are concave, and enriched in LREEs compared to HREEs (2–60 ppm La, 0.02–0.5 ppm Lu, La/Yb = 4–19) (**Supplementary Figure A7**). Trace element analyses show relatively low Zr (12–480 ppm) and Sr contents (100–870 ppm) (**Supplementary Figure A7** and **Table 3**). Low-Mg# clinopyroxene have very low Cr_2O_3 contents (<0.01 wt%), high Na_2O contents (0.94–0.96 wt% Na_2O), and are enriched in REEs compared to high-Mg# clinopyroxene (**Supplementary Figure A7**). Clinopyroxene from Kwaraha (Kw3, Kw5) are dry, with <2 ppm wt H_2O (**Figure 5** and **Table 4**).

Phlogopite is present in almost all Kwaraha samples. Phlogopites occurring as inclusions in clinopyroxene and as interstitial phenocrysts have the same composition (Mg# = 79–83, 3.1–3.6 wt% TiO_2, 13.5–14.1 wt% Al_2O_3) (**Figures 2**, **6**). They have very low F contents (0.2–0.7 ± 0.2 wt%) and phlogopite from Kw3 contains 1.57–2.12 wt% H_2O (KFT analyses). Phlogopites have variable REE (2.7–6.8 ppm La), HFSE (1.2–27.5 ppm Zr), and LILE contents (25–176 ppm Sr) (**Figure 7** and **Table 3**).

In the groundmass, nepheline microcrystals have homogeneous compositions (39.5–40.5 wt% SiO_2, 10.75–11 wt% Na_2O, 1.6–1.7 wt% FeO) (**Supplementary Table A1**). Three Fe-Ti oxide phases were identified as Ti-magnetite (18.1–18.6 wt% TiO_2, 4.5–5.6 wt% MgO), magnetite (0.03 wt% TiO_2, 0.1–0.2 wt% MgO), and rare Cr-magnetite (42.55 wt% Cr_2O_3) (**Supplementary Table A1**). Magnetites have low HFSE contents (7–75 ppm Nb, 16–39 ppm Zr). Apatite is F-rich (3–4 wt%) and Cl- (<0.02 wt%) and SO_3-poor (0.01–0.07 wt%).

Whole Rock Geochemistry

Kwaraha silicate lavas have relatively low Mg# values ranging from 67 to 56 (MgO = 15.4–9.6 wt%). These lavas have variable peralkaline indices (Na + K/Al = 0.4–1), alkali contents (Na_2O + K_2O = 2.2–6.2 wt%), and K_2O/Na_2O ratios (0.6–1.5) (**Figure 4**), and very high CaO (10.7–14.4 wt%) and moderate Al_2O_3 contents (7.4–10.1 wt%). They have variable whole-rock volatile concentrations: 0.1–2.7 wt% CO_2, 100–300 ppm S, 1400–2600 ppm F, and 33–1150 ppm Cl.

Kwaraha lavas have high incompatible element concentrations up to 350 times chondritic values. REE patterns show LREE enrichments compared to HREEs (68.2–82.2 ppm La, 0.18–0.24 ppm Lu, La/Sm = 6.9–9.7, La/Yb = 46.1–62.4) (**Figure 5A**). These lavas have high LILE (673–1225 ppm Ba, 643–1009 ppm Sr) and relatively low HFSE contents (168–259 ppm Zr) (**Figure 8B**). Trace element concentrations show negative K and Zr-Hf anomalies (**Figure 5B**), high Zr/Hf (39.2–45), Ce/Y (6.05–7.53), Nb/U (45.8–52), and Rb/Sr ratios (0.04–0.12), and low Zr/Nb (1.9–2.8) and Ba/Rb ratios (10.3–33.9). Kwaraha parasitic cones (Kw2 to Kw12) are characterized by relatively low Cr (110–367 ppm) and Ni contents (60–145 ppm).

DISCUSSION

Nephelinites erupted at Labait and Kwaraha volcanoes are among the less-differentiated and more-mafic magmas of the NTD. The high Mg# and Cr and Ni contents of olivine-bearing lavas (Mg# = 56–79, 110–1126 ppm Cr, 60–1000 ppm Ni, **Table 1**) are characteristic of primary lavas associated with rifting close to the craton (e.g., Rogers et al., 1992; Rosenthal et al., 2009; Foley et al., 2012; Baasner et al., 2016).

In the following sections, we discuss the mantle partial melting environment leading to the genesis of silica-undersaturated alkaline magmas, the role of volatiles (H_2O, CO_2) in magma differentiation and metasomatism, and the interaction between magmas and the Tanzanian lithospheric mantle. We conclude with a comparison of the characteristics of magmatism during the early stages of rift initiation in the western and

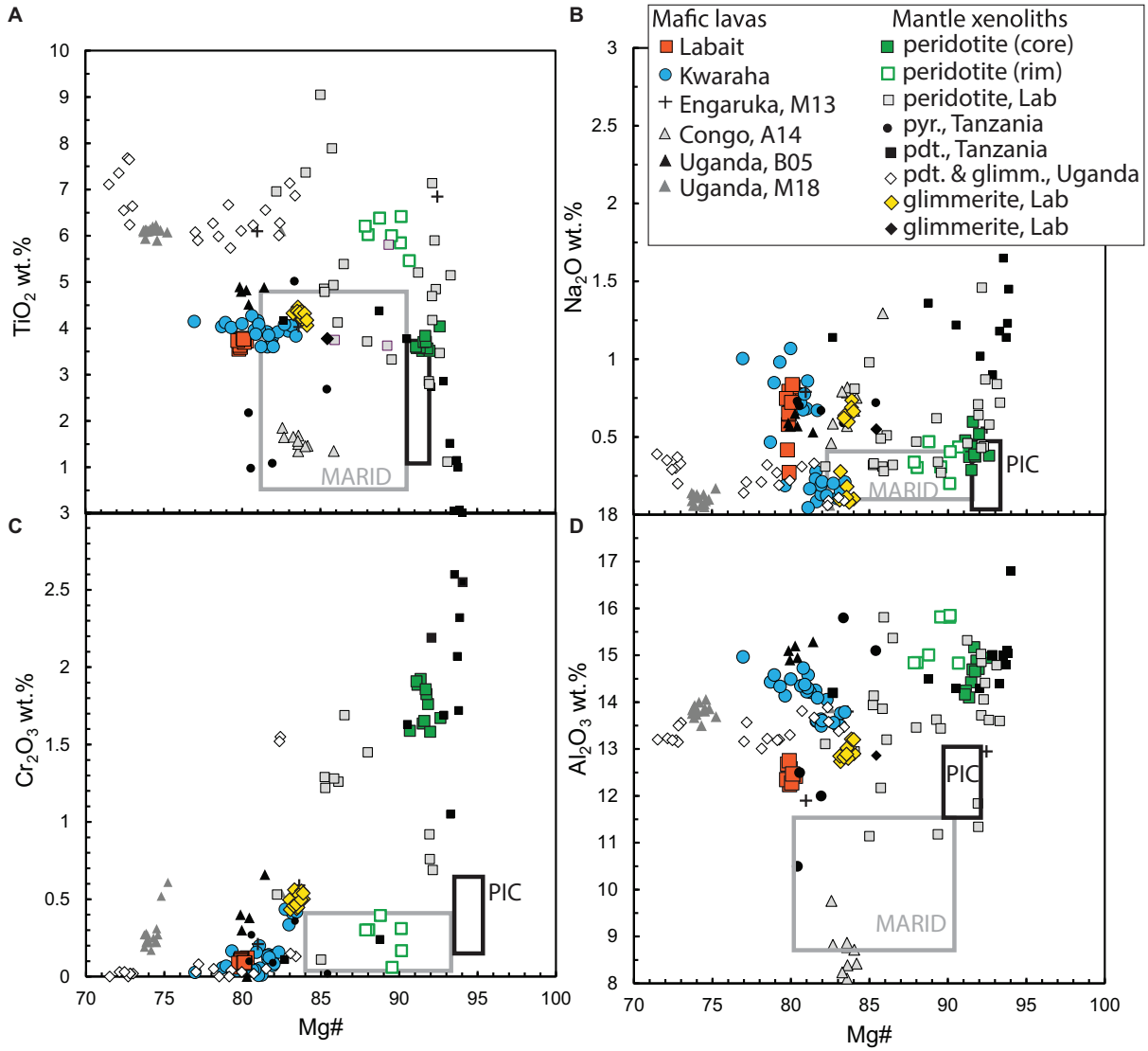

FIGURE 6 | Phlogopite compositions **(A)** TiO_2 **(B)** Na_2O, **(C)** Cr_2O_3 and **(D)** Al_2O_3 vs. Mg# from Kwaraha (blue circles) and Labait lavas (orange close squares), and glimmerite (Labx7, orange diamonds) and lherzolite xenoliths (Labx6, open orange squares). Literature data are also reported for lavas from: Engaruka (Tanzania; Mattsson et al., 2013); Nyiragongo volcano (Congo; Andersen et al., 2014); Fort Portal (Uganda; Bailey et al., 2005); Bunyaruguru volcanic field (Uganda; Muravyeva and Senin, 2018) and xenoliths from Labait (Tanzania; Lee and Rudnick, 1999; Koornneef et al., 2009) and north Tanzania (Dawson and Smith, 1988, 1992) and from Bunyaruguru volcanic field (Uganda; Muravyeva and Senin, 2018). Gray and black rectangles for phlogopite composition in MARID and PIC, respectively, from Dawson and Smith (1977); Jones et al. (1982), Kramers et al. (1983); Waters (1987), and Grégoire et al. (2002). Lab: Labait; pyr: pyroxenite; pdt: peridotite.

eastern branches of the EAR (e.g., Uganda-Rwanda and north Tanzania, respectively).

Phlogopite-Bearing Primary Alkaline Magma

Primary magmas as product of partial melting of mantle peridotite are very rare at the Earth surface as the composition of magmas can be modified in their source deeper in the mantle by crystallization and/or during ascent by interaction with or assimilation of lithospheric mantle (Huppert and Sparks, 1985; Streck et al., 2007). The compositional range observed in Labait and Kwaraha nephelinites may suggest olivine accumulation (<10%ol; Mg# = 76–79) (**Table 1** and **Figure 4**) and fractional crystallization during ascent (Kwaraha lavas with Mg# < 65), respectively (e.g., Frey et al., 1978). However, the lavas erupted at Labait and Kwaraha volcanoes are the more primitive magmas of the southern part of the NTD (i.e., Mg# > 65) and their major and trace element composition is consistent with experimental primary alkaline melt from partial melting of mantle peridotite (**Table 1** and **Figures 3**, **4**, 8; e.g., Mattsson et al., 2013; Green and Falloon, 2015).

In nephelinites, olivine and clinopyroxene are the liquidus phases and coexist with phlogopite phenocrysts. The presence

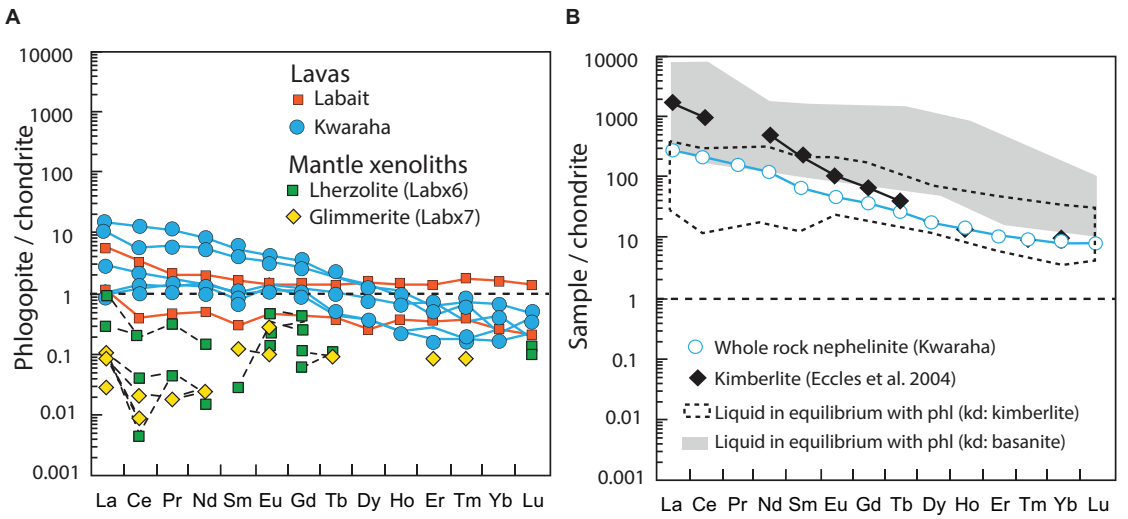

FIGURE 7 | (A) Chondrite-normalized REE patterns of phlogopite from Kwaraha and Labait lavas and lherzolite (Labx6) and glimmerite xenoliths (Labx7). **(B)** Representative chondrite-normalized whole-rock REE pattern of Kwaraha lavas, and the silicate liquids in equilibrium with phlogopite (phl) calculated using partition coefficients for kimberlite (Fujimaki et al., 1984) and basanite (Adam and Green, 2006). The chondrite-normalized REE pattern of kimberlite (Eccles et al., 2004) is shown for comparison with the calculated liquids. Chondrite and primitive mantle values from Sun and McDonough (1989).

of phlogopite in nephelinite lavas carrying phlogopite-bearing mantle xenoliths has led to the consideration that phlogopites are xenocrysts assimilated from the lithospheric mantle (e.g., Johnson et al., 1997; Lloyd et al., 2002). However, our analyses of phlogopite crystals in lavas and mantle xenoliths show that they have different major and trace element compositions, suggesting different crystallization environments. Phlogopite from Labait lavas have lower Mg# and Cr_2O_3 and Al_2O_3 contents, and higher trace element concentrations than phlogopite from glimmerite (igneous rocks mainly composed of mica) and phlogopite-bearing peridotite mantle xenoliths from the NTD (Mg# = 79–83 and 90–93, respectively, **Table 2** and **Figure 6**), suggesting that they crystallized early from primary trace-element-rich magmas. In Kwaraha nephelinites, phlogopites occur as inclusions in clinopyroxene and as phenocrysts in the groundmass (**Figure 2**) and all phlogopites have the same range of composition with high Mg# (up to Mg# = 83) suggesting an early crystallization (**Figure 2D**). The variable phlogopite compositions in Kwaraha lavas (Mg# = 83–76, **Figure 6**) correspond to their crystallization from slightly more evolved magmas with higher Al_2O_3 and trace element concentrations than phlogopite from Labait.

Using available experimentally determined partition coefficients ($D^{mineral/melt} = X^{mineral}/X^{melt}$, where X is the concentration of a given element in each phase) between phlogopite and alkaline and potassic magmas (i.e., basanite, kimberlite, lamproite; Fujimaki et al., 1984; Schmidt et al., 1999; Adam and Green, 2006, respectively), the calculated silicate liquid compositions in equilibrium with phlogopite from Kwaraha and Labait have high REE (**Figure 7B**) and trace element concentrations similar to the whole-rock nephelinite compositions. This suggests that early phlogopite crystallization occurred at the liquidus with clinopyroxene and olivine, possibly from primitive K-rich silicate liquid. These observations agree with partial melting and phase equilibria experiments in which phlogopite crystallized with clinopyroxene at high pressure (1–5 GPa) in potassic magma (Parat et al., 2010; Förster et al., 2018).

We note that the early crystallization of phlogopite in alkaline magmas may have slightly lowered the potassium content of these magmas during crystallization (5 vol% phlogopite corresponds to ~0.5 wt% K_2O). Therefore, their primary magma may have had a composition close to that of potassic melt produced by incongruent melting of a mica + amphibole + rutile + ilmenite + diopside assemblage and harzburgite at 5 GPa, which provides all the constituents for rapid growth of phlogopite and clinopyroxene (Förster et al., 2018). The high CaO contents of nephelinite NTD magmas may be related to the presence of clinopyroxene and lherzolite, rather than harzburgite, in their mantle source.

Crystallization Environment and Volatile Concentrations

Temperature, pressure, and volatile contents are key parameters controlling phase equilibria, mineral, melt, and gas compositions, and further magmatic evolution including fractional crystallization, immiscibility, and degassing processes (e.g., Carmichael and Ghiorso, 1990; Toplis and Carroll, 1995; Berndt et al., 2005). The composition of clinopyroxene in mafic magmas is strongly dependent on melt composition, pressure, and temperature during crystallization, and can be used as a geothermobarometer (e.g., Putirka, 2008; Masotta et al., 2013). Clinopyroxene and their associated bulk nephelinites have Kd (Fe^{2+}/Mg) values ranging from 0.2 to 0.41 for Kwaraha, suggesting that clinopyroxene are near equilibrium with the silicate liquid and thus suitable for calculation of the pressure

TABLE 1 | Major, volatile and trace element concentrations of the nephelinitic lavas.

Sample	Lab1	Lab2	Lab3	Kw2	Kw3	Kw4	Kw5	Kw6	Kw8	Kw10	Kw11	Kw12
SiO_2 (wt.%)	40.42	40.12	41.71	43.95	41.47	44.43	42.31	42.58	41.93	41.90	41.60	42.79
TiO_2	2.76	2.79	2.47	3.27	3.68	3.01	3.81	3.50	3.22	3.48	3.39	3.30
Al_2O_3	5.37	5.18	6.09	8.48	7.55	9.10	8.97	10.08	8.83	9.28	7.49	7.42
Fe_2O_3	14.66	15.06	13.58	14.81	15.90	12.94	16.17	15.07	14.12	14.79	15.42	14.71
MnO	0.22	0.21	0.19	0.23	0.22	0.20	0.25	0.25	0.22	0.23	0.22	0.21
MgO	28.28	24.81	24.91	12.78	15.44	12.63	10.92	9.66	13.00	12.56	15.05	15.22
CaO	5.00	7.11	7.36	13.68	12.30	14.40	10.77	12.61	13.55	12.75	13.81	12.68
Na_2O	1.22	2.50	1.63	0.85	0.56	1.87	3.56	3.64	2.65	2.64	1.22	1.46
K_2O	1.34	1.65	1.49	1.30	2.23	1.19	2.63	2.13	1.83	1.70	1.19	1.61
P_2O_5	0.74	0.58	0.48	0.65	0.64	0.24	0.61	0.49	0.64	0.66	0.60	0.58
F (ppm)	1500	1700	1100	–	1900	1600	1400	2100	–	2000	2200	2600
Cl (ppm)	44	71	49	–	33	660	1150	550	–	99	89	72
S (ppm)	260	200	200	270	222	148	140	220	300	100	100	100
Total	100	100	100	100	100	100	100	100	100	100	100	100
Mg#	79.26	76.54	78.42	63.1	65.81	65.9	57.22	55.95	64.59	62.7	65.91	67.21
Cr (ppm)	756	495	1126	294	366	246	141	110	334	247	368	335
Ni	827	1000	890	125	143	102	60	64.6	90.4	74.9	145	121
Cu	117	118	115	171	168	150	262	219	173	182	198	193
Cs	0.21	0.15	2.62	0.26	0.28	0.27	0.44	0.36	0.34	0.27	0.24	0.11
Rb	44.9	51	64.7	48.4	74.3	36.1	58.5	45.4	61.3	41.9	48	67.2
Ba	595	621	551	775	801	1225	673	1166	812	854	750	689
Th	7.34	8.37	7.99	7.83	8.06	8.51	9.7	9.79	10.7	9.73	9.89	8.99
U	1.48	1.73	1.45	1.7	1.72	1.68	2.01	2.05	2.02	2.22	4.59	1.89
Nb	78.9	90.4	78.3	86	82.4	81	104	107	101	102	87.3	95.7
Ta	5.4	5.13	4.8	5.96	5.7	5.49	7.45	7.73	6.94	5.41	5.42	6.02
La	64.9	68.3	62.7	68.2	68.2	69.2	76.6	76.8	82.2	75.7	80.8	77.9
Ce	123	120	111	128.6	130.2	130.5	144.8	142.8	152	130.2	132.5	128
Pb	2.99	3.85	7.04	3.06	4.16	4.5	8.09	6.22	8.31	9.8	5.35	0.64
Pr	13.7	13.4	12.5	14.4	14.9	14.8	16.3	15.8	16.7	14.6	14.1	13.8
Sr	840	754	853	1009	643	1108	811	931	989	934	937	867
Nd	49.7	49.6	46.3	53.7	55.9	54.9	59.9	58.9	60.9	54.1	51.6	50.6
Zr	178	183	168	180	207	226	255	259	220	255	168	190
Hf	4.16	3.97	3.94	4.47	4.97	5.28	6.52	6.43	5.34	5.68	4.14	4.63
Sm	7.91	7.73	7.34	9.13	9.76	9.57	10.65	10.27	10.47	8.96	8.35	8.33
Eu	2.14	2.27	2.1	2.53	2.64	2.71	2.84	2.91	2.86	2.75	2.51	2.45
Gd	6.07	7.81	7.37	7.15	7.48	7.45	8.37	8.08	7.96	9.49	8.83	8.81
Tb	0.787	0.799	0.77	0.941	0.99	1.012	1.12	1.103	1.077	1.041	0.936	0.953
Dy	3.34	3.54	3.47	4.34	4.51	4.62	5.25	5.19	5.22	4.91	4.41	4.52
Y	14.2	14.3	13.1	19.8	19.8	20.3	23.3	23.6	23.4	21.2	17.6	19.3
Ho	0.55	0.58	0.57	0.78	0.79	0.81	0.91	0.93	0.93	0.84	0.75	0.78
Er	1.26	1.31	1.25	1.81	1.71	1.9	2.06	2.08	2.01	1.94	1.71	1.8
Tm	0.16	0.16	0.15	0.25	0.22	0.26	0.28	0.3	0.29	0.25	0.22	0.23
Yb	0.91	0.96	0.91	1.47	1.35	1.5	1.66	1.62	1.68	1.5	1.29	1.42
Lu	0.14	0.13	0.12	0.2	0.19	0.22	0.24	0.24	0.24	0.21	0.18	0.2

*Mg# = Mg/(Mg+Fe)*100; bdl, below detection limit.*

and temperature conditions during their crystallization. This is corroborated by clinopyroxene trace element concentrations, which indicate equilibrium with the whole rock based on experimental partition coefficients for alkaline magmas (Adam and Green, 2006; **Supplementary Figure A8**). Assuming clinopyroxene-melt equilibrium and using the thermobarometer of Masotta et al. (2013; σ = 50°C, 150 MPa), we estimate the temperature and pressure during crystallization to have been 1170–1290°C and 200–1080 MPa for Kwaraha lavas (**Supplementary Figure A9**). Simonetti et al. (1996) proposed a correlation between the Al^{VI}/Al^{IV} ratio of clinopyroxene and their crystallization pressure, and the high clinopyroxene Al^{VI}/Al^{IV} ratios (0.89–0.56) from Kwaraha are consistent with crystallization at 1000 MPa.

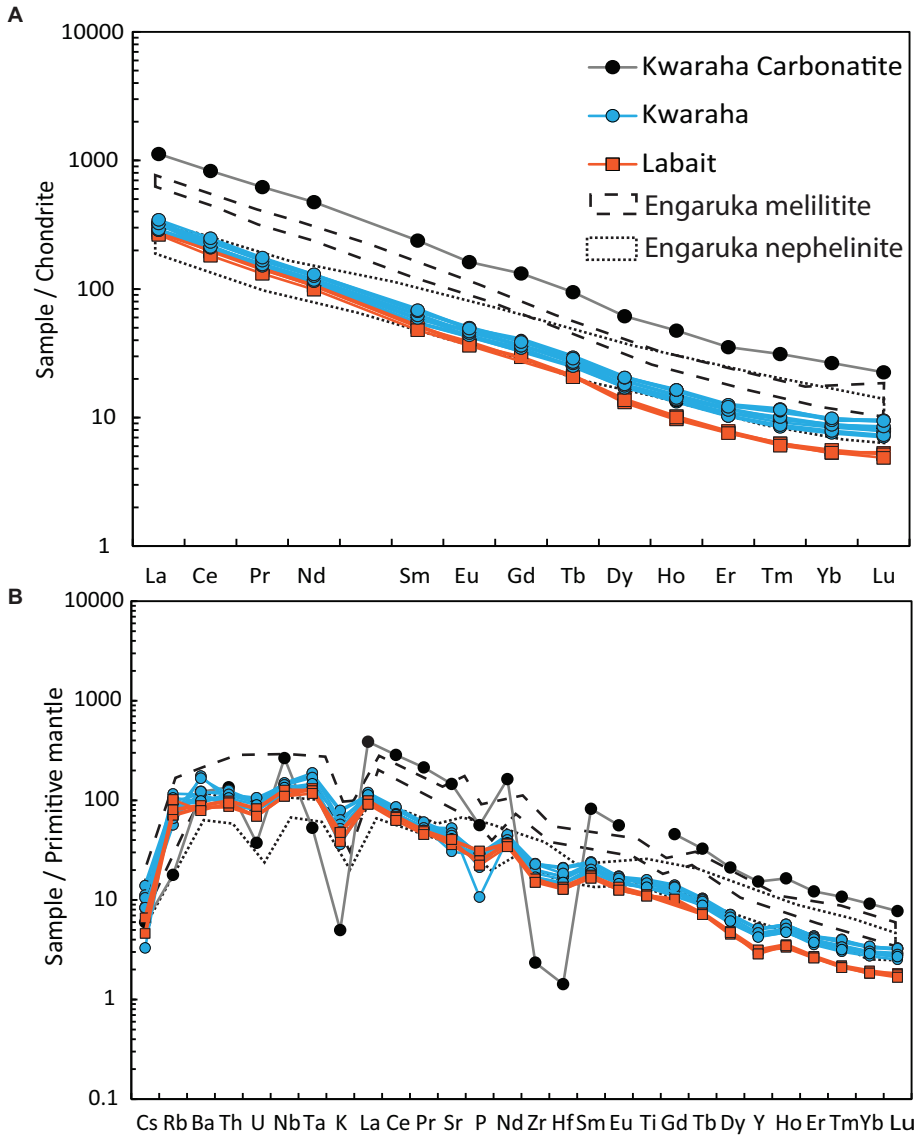

FIGURE 8 | (A) Chondrite-normalized REE contents and **(B)** primitive mantle-normalized trace element compositions of Kwaraha and Labait nephelinites (symbols as in **Figures 3**, **4**) and the Kwaraha carbonatite (black circles). Primitive mantle and chondrite values from Sun and McDonough (1989). Engaruka melilitites and Engaruka nephelinites from Mattsson et al. (2013) are also reported.

Volatiles such as CO_2 and H_2O affect the conditions of partial melting (e.g., Dasgupta et al., 2007; Baasner et al., 2016), play a fundamental role during magmatic evolution and ascent, and control eruptive style (e.g., Oppenheimer et al., 2003; Berndt et al., 2005). The presence of phlogopite in Kwaraha and Labait lavas suggests that the silicate melts were H2O-bearing at the time of phlogopite crystallization (1.57–2.12 wt% H2O in phlogopite, KFT method). However, the abundant water in crystal lattice of phlogopite (OH site) prevents us from quantifying precisely the amount of water present in the melt (i.e., non-Henrian behavior). In experimental study, hydroxyl-rich phlogopite with 4.3 wt.% H_2O crystallized from hydrous melt with 3.1 wt.% H_2O at 1250°C and 3 GPa (Condamine et al., 2016; calculated D_{H2O} = 1.4), suggesting that 1.12–1.4 wt.% H_2O may have been present in the melt at the time of phlogopite crystallization.

Only nominally anhydrous minerals (NAMs) such as olivine and clinopyroxene incorporate trace concentrations of hydrogen that can be used to determine the H_2O content of the silicate melt during their crystallization ($D^{clinopyroxene/melt}$ = 0.01–0.013, $D^{olivine/melt}$ = 0.0013; Aubaud et al., 2004; Hauri et al., 2006). The measured water contents are very low: < 1 ppm wt H_2O in clinopyroxene and olivine from Kwaraha lavas (**Figure 5**) and 3–6 ppm wt H_2O in olivine from Labait. Using the partition

TABLE 2 | Representative major element compositions of minerals.

Sample	Lab3	Lab1	Labx6	Labx7	Kw3	Kw3	Kw3	Kw5	Kw11	Kw11
Mineral	**ol**	**phl**	**phl**	**phl**	**phl**	**ol**	**cpx**	**cpx**	**cpx**	**cpx**
SiO_2	41.17	39.97	38.50	38.57	38.30	40.96	52.12	52.97	53.50	50.15
TiO_2	0.07	3.26	3.52	4.23	3.61	0.06	0.85	0.58	0.55	1.50
Al_2O_3	0.03	12.43	14.71	13.21	14.03	0.03	2.03	1.33	1.37	2.39
FeO	11.12	8.89	3.48	7.33	7.69	11.35	5.49	4.34	3.96	9.09
MnO	0.19	0.04	0.03	0.03	0.04	0.19	0.11	0.07	0.06	0.20
MgO	46.42	19.77	22.33	21.38	20.02	46.69	15.04	16.22	15.85	11.68
CaO	0.53	0.01	0.01	0.02	0.05	0.29	23.53	23.31	22.32	23.03
Na_2O	0.00	0.76	0.52	0.69	0.08	0.00	0.84	0.66	0.88	0.94
K_2O	0.00	9.89	10.44	10.05	10.68	0.01	0.00	0.01	0.00	0.01
Cr_2O_3	0.05	–	1.58	0.51	–	0.07	0.03	0.49	1.11	0.00
NiO	0.18	–	–	–	–	0.25	0.01	0.01	0.05	0.00
F	–	0.78	0.39	0.23	0.42	–	–	–	–	–
Total	99.78	95.84	95.51	96.25	94.92	99.90	100.05	99.97	99.64	99.01
Mg#	88.1	79.8	92.0	83.9	82.2	87.8	82.9	86.9	87.7	69.6
Numbers of ions on the basis of										
	4O	**24O**				**4O**	**6O**			
Si	1.02	5.68	5.48	5.54	5.50	1.01	1.91	1.94	1.96	1.90
Al^{IV}	–	2.08	2.47	2.24	2.38	–	0.09	0.06	0.04	0.10
Al^{VI}	–	0.00	0.00	0.00	0.00	–	0.00	0.00	0.02	0.00
Al tot	0.00	–	–	–	–	0.00	–	–	–	–
Ti	0.00	0.35	0.50	0.61	0.39	0.00	0.02	0.02	0.02	0.04
Fe^{2+}	–	–	–	–	–	–	0.07	0.06	0.11	0.20
Fe^{3+}	–	–	–	–	–	–	0.10	0.07	0.01	0.08
Fe tot	0.18	1.06	0.41	0.88	0.92	0.23	–	–	–	–
Mn	0.00	0.00	0.00	0.00	0.00	0.00	0.00	0.00	0.00	0.01
Mg	1.78	4.19	4.74	4.58	4.29	1.72	0.82	0.88	0.87	0.66
Ca	0.00		0.00			0.01	0.92	0.91	0.88	0.93
Na	–	0.21	0.14	0.19	0.02	–	0.06	0.05	0.06	0.07
K	–	1.79	1.86	1.84	1.96	–	–	–	–	–
Ni	0.01	–	–	–	–	0.00	–	–	–	–
Cr	–	–	0.18	0.06	–	–	0.00	0.01	0.03	0.00
OH	–	3.65	3.82	3.90	3.81	–	–	–	–	–
F	–	0.35	0.18	0.10	0.19	–	–	–	–	–
Total	3	19.36	19.78	19.94	19.43	3	4	4	4	4

ol olivine, cpx clinopyroxene, phl phlogopite.

coefficients of Hauri et al. (2006), the water content in the nephelinite melt was 0.2–0.5 and <0.01 wt% H_2O during olivine and clinopyroxene crystallization, respectively (**Table 4**). However, calculated H_2O melt content for Labait is up to 0.5 wt% H_2O, consistent with the estimation from xenoliths suggesting that they were carried by H_2O-poor mafic magmas (Hui et al., 2015). It should be noted that these partition coefficients were determined for ol-clinopyroxene-melt equilibria in basaltic melt, and that no experimental data exists for potassic melts bearing hydrous minerals. The presence of phlogopite may have strongly influenced the distribution of water between anhydrous minerals and the melt, with H_2O being preferentially incorporated into phlogopite, and our estimated water contents in the melt should be considered minimum values. Petrographic observations strongly suggest an early crystallization of phlogopite, before clinopyroxene, whereas both phlogopite and NAMs data allow us to discuss the H_2O content in primary magmas. In the primary alkaline melt, water content was high enough to allow phlogopite crystallization and stabilize this hydrous mineral through all the magmatic stage. Due to uncertainties on distribution of water in NAMS in presence of hydrous minerals, we can assume that calculated H_2O content from NAM's mineral is a minimal value. Based on experimental data, H_2O content of the melt during phlogopite crystallization could have reached 1.4 wt% H_2O at $P > 3$ GPa (Condamine et al., 2016). Although primary melts from Labait and Kwaraha are hydrated, the water content was probably not high enough to favor phlogopite crystallization over olivine (Foley, 1993).

CO_2 contents in silicate melts are generally investigated through melt inclusion studies (e.g., Métrich and Wallace, 2008; Hudgins et al., 2015; Baudouin et al., 2018). The lack of melt inclusions in minerals from Labait and Kwaraha lavas prevents

TABLE 3 | Trace element compositions of minerals.

Sample mineral	Lab1 ol	Lab1 phl	Labx6 phl	Labx7 phl	Kw3 Phl	Kw3 ol	Kw3 cpx	Kw5 cpx	Kw5 cpx	Kw11 cpx	Kw11 cpx
Cs	0.01	3.32	3.27	1.89	1.94	0.01	0.18	0.01	0.01	< 0.01	<0.01
Rb	0.06	558	204	347	314	0.09	0.5	0.03	0.03	< 0.01	<0.01
Ba	0.14	2383	3095	911	2014	0.11	3.45	0.11	0.1	0.06	0.05
Th	0.00	0.01	0.00	–	–	0.00	0.21	0.01	0.04	0.02	0.02
U	0.02	1.5	–	–	0.09	–	< 0.01	–	–	–	< 0.01
Nb	0.36	15.8	22.05	9.93	6.67	0.05	2.62	0.92	0.4	0.19	0.28
Ta	0.02	1.42	2.74	0.81	0.47	0.00	0.34	0.13	0.14	0.04	0.02
La	0.01	48.6	0.07	0.02	0.62	0.01	49.8	4.57	4.75	3.29	8.12
Ce	0.09	29.3	0.126	0.014	0.11	0.01	148	16.0	15.5	11.0	17.5
Pr	0.00	5.61	–	–	0.04	0.00	24.3	2.69	2.6	1.87	2.33
Sr	0.08	418	33.2	25.9	142	0.02	790	216	155	124	303
Nd	0.03	26.5	0.01	0.01	0.22	0.04	127	12.7	12.6	9.33	10.1
Zr	0.55	49.2	18.08	5.42	8.72	0.73	419	320	110	49.2	110
Hf	0.01	0.9	0.45	0.196	0.12	0.01	23.9	9.62	5.65	2.41	4.13
Sm	0.01	6	–	–	0.05	0.02	31.2	2.72	3.07	2.49	1.94
Eu	0.01	2.66	0.01	0.02	0.04	0.01	10.7	0.86	0.91	0.72	0.60
Gd	0.07	10.8	0.01	0.02	0.23	0.08	23.2	2.34	2.65	2.02	1.63
Tb	0.01	2.21	–	–	0.04	0.00	3.66	0.29	0.33	0.26	0.23
Dy	0.01	13.9	–	–	0.31	0.05	16.1	1.71	1.91	1.32	1.10
Y	0.13	141	0.20	0.06	3.76	0.45	58.4	6.26	6.08	4.62	4.09
Ho	0.01	3.75	–	–	0.09	0.02	2.66	0.29	0.28	0.20	0.17
Er	0.01	12.7	–	–	0.30	0.05	6.04	0.73	0.63	0.42	0.43
Tm	0.00	2.11	–	–	0.05	0.02	0.76	0.12	0.08	0.05	0.06
Yb	0.04	10.9	–	–	0.31	0.13	2.56	1.27	0.47	0.32	0.43
Lu	0.01	1.63	–	–	0.04	0.04	0.49	0.28	0.07	0.05	0.09

Ol, olivine; cpx, clinopyroxene; phl, phlogopite.

TABLE 4 | Water contents in olivine and cpx, and those calculated for their associated parental melts.

Sample	Mineral	ppm wt H_2O	$H/10^6$ Si	Area[a]	Melt[b] (wt% H_2O)
Lab1	Olivine	5.3	86.472	44.8	0.41
Lab1	Olivine	2.5	41.14	18.4	0.19
Lab1	Olivine	5.5	89.17	47.2	0.42
Lab1	Olivine	4.3	70.655	32.4	0.33
Lab1	Olivine	4.9	80.375	39.6	0.38
Lab1	Olivine	6.6	108.09	67.2	0.51
Lab1	Olivine	5.9	96.529	54.4	0.45
Kw3	Olivine	1.2	19.262	6.7	0.09
Kw3	Olivine	1.7	27.859	9.3	0.13
Kw5	Olivine	0.7	11.619	4.6	0.05
Kw5	Olivine	0.6	10.429	4.3	0.05
Kw3	Clinopyroxene	0.5	7.93	3.7	0.004
Kw3	Clinopyroxene	1.7	26.988	10.3	0.013
Kw3	Clinopyroxene	1.5	25.028	9.6	0.012
Kw5	Clinopyroxene	0.4	7.02	3.3	0.004
Kw5	Clinopyroxene	0.4	6.35	3.1	0.004
Kw5	Clinopyroxene	0.3	5.703	2.8	0.003

[a]*Integrated unpolarized absorbance normalized to 1 cm thickness.* [b]*Melt water content calculated using* $D^{olivine/melt}$ *and* $D^{clinopyroxene/melt}$ *from Aubaud et al. (2004) and Hauri et al. (2006).*

us from precisely constraining the CO_2 content of the nephelinite magmas. However, northern Tanzania contains some of the most concentrated carbonatite magmatism on Earth (e.g., Dawson, 2012) and the occurrence of calciocarbonatite lava (Kw1) at Kwaraha volcano strongly suggests the presence of abundant CO_2 in the primary alkaline magmas. CO_2 solubility in alkaline magmas (e.g., melilitite, phonolite) was experimentally calibrated at 1.5–2 GPa, and strongly depends on the ratio of non-bridging oxygens to tetrahedrally coordinated anions (NBO/T) in the melt (Brooker et al., 2001; Moussallam et al., 2015). Based on the observed compositions of nephelinite lavas (NBO/T = 1.4–1.67 for Labait and 0.93–1.26 for Kwaraha), their CO_2 solubilities (i.e., the maximum amount of CO_2 that can be dissolved in the magma) range from 7.5 to 15.8 wt% CO_2 (**Supplementary Figure A10**). The primary magma from Labait evolved to a Mg-poor nephelinitic liquid containing up to 6 wt% CO_2 at 800 MPa (Hanang volcano; Baudouin et al., 2018); CO_2 contents of Labait nephelinites may indicate that fractional crystallization and immiscibility buffered the CO_2 content during differentiation ($<$6 wt% CO_2).

Partial Melting of Metasomatized Deep Mantle

Alkaline mafic lavas such as melilitites and nephelinites represent more primitive magmas erupted in intracontinental settings, and are characterized by silica-undersaturation and very high Mg contents (Dasgupta et al., 2007; Foley et al., 2012). Their high incompatible element concentrations and strong REE fractionations (Ivanikov et al., 1998; Platz et al., 2004; Keller et al., 2006) have been proposed to result from very low degrees of partial melting of CO_2-bearing lherzolite (Green and Falloon, 1998; Foley et al., 2009, 2012; Foley and Fischer, 2017) or the partial melting of peridotite with contributions from recycled oceanic crust (e.g., Hofmann, 1988) or pyroxenite (Eggler and Holloway, 1977; Dasgupta et al., 2007; Baasner et al., 2016).

Around the Tanzanian craton, nephelinite volcanoes are concentrated at the propagating tips of the rift and mafic and carbonate-rich alkaline melts are associated with thick lithosphere (Foley and Fischer, 2017). The presence of deep garnet-bearing mantle xenoliths in Labait scories indicate that partial melting occurred at least at 150 km (Lee and Rudnick, 1999).

Geochemical modeling results of the partial melting of mantle peridotite to produce Labait and Kwaraha nephelinite magmas corroborate the presence of refractory HREE-rich minerals such as garnet in the mantle source (**Figure 9**). Trace elements such as Y and Rb are compatible in garnet and phlogopite, respectively, which can account for the high Ce/Y ($>$5) and Rb/Sr ratios in the nephelinite melt (Rogers et al., 1992; Platz et al., 2004; Mana et al., 2015). Partial melting of a garnet peridotite with 62% olivine, 16% opx, 12% clinopyroxene and 10% garnet (theoretical mineral assemblage in mantle from Sun and McDonough, 1989) produces melts with high Ce/Y ($\sim$3), low Rb/Sr ($<$0.04), and low Zr/Hf ratios that cannot represent the composition of nephelinite (i.e., Ce/Y $>$ 5, Rb/Sr $>$ 0.04, Zr/Hf = 39.2–46). The high Rb/Sr ratios ($>$0.04) in the nephelinites strongly suggest a contribution of phlogopite (Rogers et al., 1992; Platz et al., 2004), whereas their high Zr/Hf ratios indicate the contribution of a carbonated source (Rudnick et al., 1993). We modeled the partial melting of carbonatite-free and carbonated (0.3 and 1% carbonatitic component) garnet-rich and phlogopite-bearing peridotite mantle (62% olivine, 16% opx, 10% clinopyroxene, 10% garnet, 2% phlogopite, proportion modified from Sun and McDonough, 1989), as well as a natural garnet-bearing xenolith from Lashaine volcano in the north part of the NTD (Gibson et al., 2013).

The best fit to the observed data suggests that nephelinites result from a very low degree of partial melting ($<$1%) with non-modal fractional melting (**Figure 9** and **Supplementary Figure A11**). The low volumes of melts ($<$1%) is generally assume to be motionless in the mantle rocks due to their small permeability and wetting angle characteristics (Maumus et al., 2004). However, recent study based on physical properties and melt-rock reaction suggest that small volume of melts (i.e., 0.75%) could be extracted from the mantle (Soltanmohammadi et al., 2018). The extraction of low volume melt will be effective for a melt with high content in alkaline and volatile elements (Keller and Katz, 2016; Soltanmohammadi et al., 2018), the volatile content being a key parameter to enhance the melt extraction process due to their effect on the melt viscosity properties (Condamine and Médard, 2014; Gardès et al., 2020). In Labait and Kwahara lavas, early phlogopite crystallization suggests that the primary magmas have higher K content than the erupted lavas (nephelinites), and high volatile contents, especially in CO_2, allowing low melt volume 0.5–1 vol% to be extracted from the mantle (Keller and Katz, 2016; Gardès et al., 2020).

Small amounts of carbonate in the source reproduce the high Zr/Hf fractionation observed in Labait lavas (Zr/Hf = 42.6–46) (**Figure 8**). The trace element variability of lavas from Labait and Kwaraha may suggest that the lavas originate from different degrees of partial melting (0.2–1%) and/or variable carbonate components in their mantle sources (0.3%, **Figure 9B**). The mantle source may be homogeneous (i.e., phlogopite-bearing lherzolite) or mixed heterogeneous source (i.e., 90% phlogopite-free lherzolite + 10% phlogopite-pyroxenite), as suggested by isotopic signatures (Paslick et al., 1996; Aulbach et al., 2011), both leading to similar trace element characteristics in primary melts. It should be noted that pyroxene and phlogopite (i.e., mica pyroxenite) as main component of the mantle source would lead to the genesis of highly alkaline melt with trace element content higher than those reported in Labait and Kwaraha lavas.

Using the empirical equation of Albarède (1992), calibrated for partial melting producing basaltic melts, the SiO_2 and MgO contents of the primary melts suggest that the melting pressure was 110–130 km (3.7–4.3 GPa) for Kwaraha, and 150 km (5 GPa) for Labait, below or close to the lithosphere-asthenosphere boundary (LAB at 146 km close to the Tanzanian craton beneath Labait and 135 km beneath Kwaraha, Craig et al., 2011; **Figure 10**). The depth and temperature of partial melting are consistent with (i) the presence of garnet in the mantle source ($>$90 km; McKenzie and O'Nions, 1991; Sato et al., 1997), (ii) the presence of mantle xenoliths equilibrated at 100–147 km depth (3.2–4.9 GPa; Lee and Rudnick, 1999), and

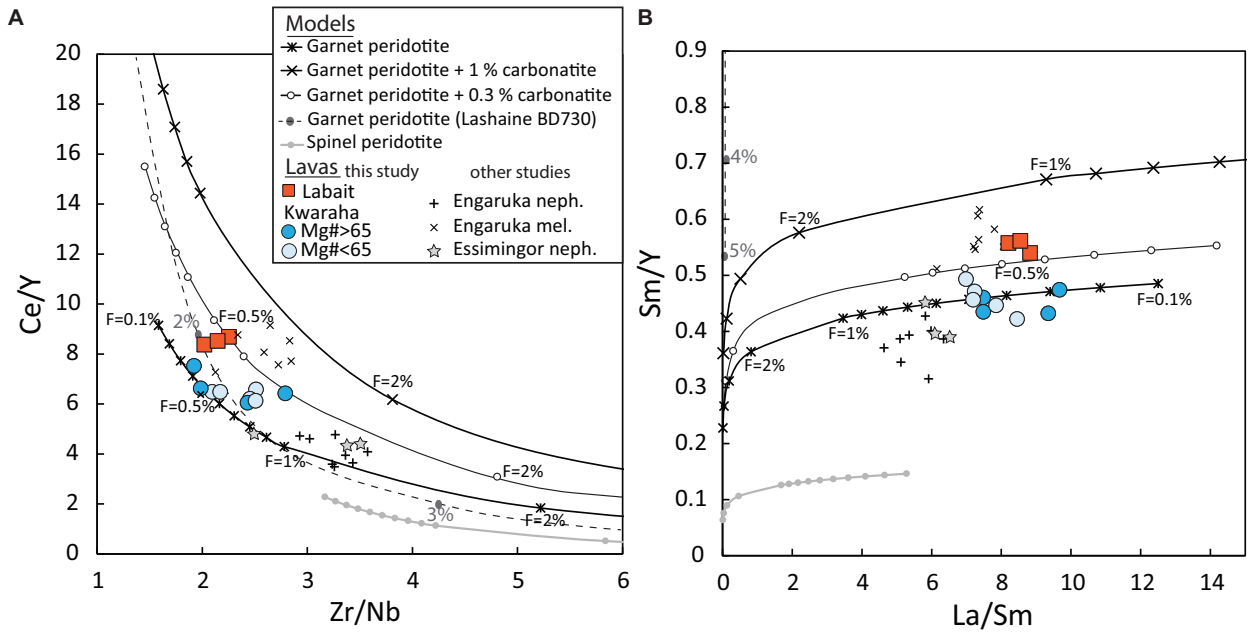

FIGURE 9 | Geochemical model of primary mantle melting for Kwaraha and Labait lavas using **(A)** Ce/Y vs. Zr/Nb ratios and **(B)** Sm/Y vs. La/Sm ratios. Partial melting of a garnet peridotite (62% olivine, 16% opx, 10% clinopyroxene, 10% garnet, and 2% phlogopite), spinel peridotite and garnet peridotites with the addition of 0.3 and 1% carbonatite (Kw1 composition) was modeled with no modal fractional melting. Partial melting of a garnet-bearing xenolith from Lashaine volcano (sample BD730 from Gibson et al., 2013) has also been modeled. The degree of melting (F) is indicated for each composition. Nephelinites (neph.) and melilitites (mel.) from Engaruka-Natron basin (Mattsson et al., 2013) and nephelinites from Essimingor (Mana et al., 2012) are also reported. Mafic nephelinites from Kwaraha (Mg# > 65) are reported in blue circles, and less mafic lavas from Kwaraha (Mg# < 65, **Table 1**) are reported in light blue circles.

(iii) magnetolleruric data by Selway et al. (2014) suggesting that beneath Labait, the geotherm was initially cratonic at 44 mW/m^2, before been impacted by the plume ascent, increasing the mantle temperature of 300°C at 5 GPa, which may lead to melting of fertile lherzolite (**Figure 10**).

The presence of phlogopite in Kwaraha and Labait magmas indicates that the asthenospheric mantle source is hydrated, which may considerably decrease the solidus temperature (e.g., Green et al., 2014). The water content of the nephelinite magma estimated from the water content of olivine and clinopyroxene was 0.2–0.5 wt% H_2O (**Table 4**). Considering 1% partial melting, the garnet-rich and phlogopite-bearing peridotite source may have contained around 300 ppm H_2O (Novella et al., 2015; Demouchy and Bolfan-Casanova, 2016).

Most of the experimental studies performed to determine the depth of partial melting and the composition of primitive alkaline magmas have been carried out in K- and H_2O-free systems, that are not relevant for our phlogopite-bearing magmas (CMAS-CO_2; **Figure 10**; e.g., Green and Falloon, 1998; Gudfinnsson and Presnall, 2005). On the other hand, the experiments that investigated the partial melting in the presence of K_2O and water for alkaline magmas in the KMASH system at P < 4.5 GPa and T < 1300°C (phl = phl+grt+melt; Yoder and Kushiro, 1969; Sato et al., 1997; Trønnes, 2002), KCMASH system at 3.5–17 GPa and T < 1400°C (phl+cpx = phl+cpx+grt+ol+melt; Luth, 1997) and KNCMASH system at 4–9.5 GPa and T < 1200°C (phl+cpx+opx = amph+grt+ol+melt; Konzett and Ulmer, 1999) were not performed to account for the presence of garnet (gt) and phlogopite (phl) in lherzolite. Recently, experiments by Condamine et al. (2016) show that melting of phlogopite-garnet lherzolite leads to the reaction phl+cpx+grt = olivine+opx+melt at 3 GPa and 1300°C and forms foiditic to trachy-basaltic melts (44–47 wt% SiO_2, Na_2O+K_2O = 5.2–11.3 wt%) for various degree of melting (F = 0.008–0.255) and alkaline contents. However, the experimental melts from partial melting of phlogopite-bearing lherzolite have higher alkali and silica contents compared to the nephelinite magmas. Similarly, partial melting of water- and carbonate-bearing and phlogopite-free lherzolite (Dasgupta et al., 2007) and carbonate-bearing and phlogopite-rich MARID (Mica-Amphibole-Rutile-Ilmenite-Diopside; Förster et al., 2018) or potassium enriched pyrolite (Foley et al., 2009) at 3–5 GPa do not reproduce the K_2O, CaO, and TiO_2 concentrations of nephelinite magmas (**Figures 3**, 4).

The presence of carbon in mantle source is an important parameter to consider for partial melting at the lithosphere-asthenosphere boundary because (i) it induces a decrease of the solidus temperature of peridotite (Dasgupta et al., 2007) and (ii) below 5 GPa (below LAB), carbon is stable as graphite and it will be oxidized at 4–5 GPa to produce carbonate melt (redox melting, **Figure 10**; Green and Falloon, 1998; Stagno et al., 2013; Hammouda and Keshav, 2015). Experiments of partial melting of CO_2- and phlogopite-bearing garnet peridotite at high pressure (>4–5 GPa) would help to better understand the

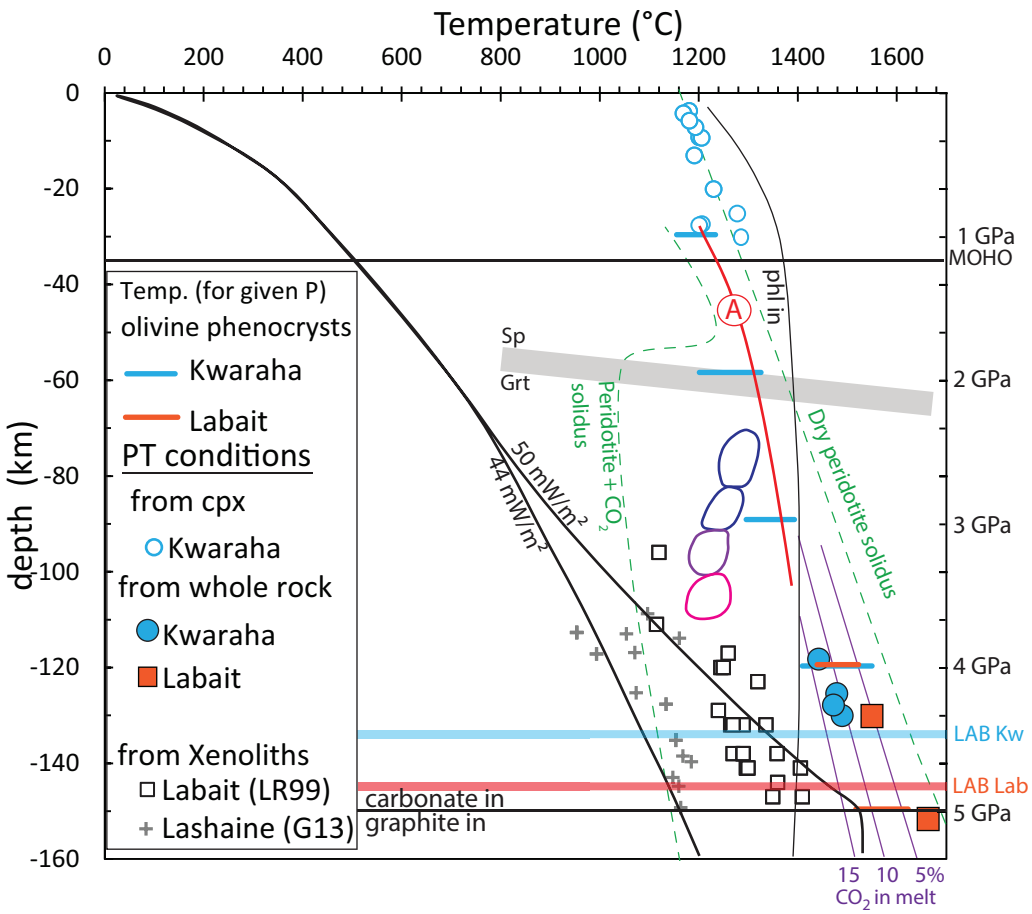

FIGURE 10 | P-T conditions of clinopyroxene crystallization calculated from the clinopyroxene-liquid thermobarometer (Putirka, 2008) for Kwaraha (Mg# > 65) and P-T conditions of partial melting (Albarède, 1992) for Kwaraha and Labait lavas. P-T conditions for Labait and Lashaine mantle xenoliths are from Lee and Rudnick (1999) LR99 and Gibson et al. (2013) G13, respectively. Crystallization temperatures of olivine are represented by color bars (blue: Kwaraha, and orange; Labait; calculation from Putirka, 2008). We include the dry peridotite and peridotite+CO_2 solidi and melt CO_2 isopleths with CO_2 content in weight percent from Dasgupta et al. (2013), the spinel-garnet boundary from Lee et al. (2000), and the lithosphere-asthenosphere boundary (LAB) from Craig et al. (2011). The curve of phlogopite stability (phl) correspond to experiments (KMASH) from Yoder and Kushiro (1969); Sato et al. (1997), and Trønnes (2002). The reaction (A) F-phl+cpx+grt = ol+opx+melt has been determined from melting experiments of phlogopite-garnet peridotite by Condamine et al. (2016). Cratonic geotherm (44 mW/m^2) and geotherm modified by plume thermal anomaly are also reported (Selway et al., 2014), as well as the different melt types produced by low partial melting of CMAS ± H_2O and CO_2: Colored balloons represent P and T conditions of partial melting for basanite (blue balloon), nephelinite, melilitite, and leucitite melt compositions (pink balloon) (Frey et al., 1978; Adam, 1990; Green and Falloon, 1998).

melting conditions of primary nephelinite melt as observed at Labait and Kwaraha volcanoes in the southern part of the NTD.

Melt-Rock Interaction and Lithospheric Metasomatism

Percolation of CO_2- and water-bearing alkaline nephelinite magmas from the LAB through the lithospheric mantle may have induced metasomatism and phlogopite crystallization in garnet and spinel lherzolite and glimmerite lithologies. The large variety of mantle xenoliths sampled by nephelinite lavas at Labait and other localities of NTD strongly indicates that the lithospheric mantle beneath the Tanzanian Craton edge is highly heterogeneous, including fertile and refractory mantle peridotite (i.e., Cr spinel with high Cr#; Cr# up to 94), and metasomatized amphibole- and/or phlogopite-bearing peridotite (Dawson and Smith, 1988; Lee and Rudnick, 1999; Koornneef et al., 2009; Gibson et al., 2013; Baptiste et al., 2015).

The study of magmatic phlogopite in nephelinite and mantle phlogopite in xenoliths from Labait and Kwaraha corroborates previous studies that established the nature and the timing of the metasomatism events. Xenoliths from Labait, Lashaine, Pello hill, and Eledoi (Natron basin) suggest the percolation of a H_2O-rich metasomatic agent within the lithospheric mantle and the presence of heterogeneous lithosphere related to different metasomatic events (Jones et al., 1983; Dawson and Smith, 1988; Rudnick et al., 1993; Koornneef et al., 2009; Baptiste et al., 2015). NAMS minerals in lithospheric peridotites have a low water content (<50 ppm wt H_2O whole rock peridotite; Baptiste et al., 2015; Hui et al., 2015) although the presence of hydrous minerals as amphibole and phlogopite indicates the

presence of K_2O-MgO-H_2O-rich silicate melt in the lithosphere. The composition of phlogopite in mantle xenoliths from Labait (i.e., glimmerite, core, and rim of phlogopite in lherzolite, **Figure 6**) indicate at least 3 metasomatic events within the continental lithosphere. Multiple stage of metasomatism in the lithosphere beneath Labait have already been suggested from textural, chemical and isotopic data (Koornneef et al., 2009): Phlogopite, Cr-rich diopside and spinel pockets were produced by an old metasomatism event (i.e., Pan-African Orogeny, 610–650 Ma) associated with a liquid rich in Ni, Cr, Na, K, H_2O, Ba, Fe, Ti. Glimmerite lithologies could be formed by recent metasomatism (rift event) and melt differentiation in veins in the lithosphere, induced by the percolation of nephelinite liquid rich in K, Fe, Ti, and poor in Cl, Mg, Al, Ba (**Figure 10** and **Table 3**). Rift related metasomatism event was previously suggested as anhydrous from textural observation for a spinel lherzolite (Koornneef et al., 2009). However, it can be noted that glimmerite xenoliths (or glimmerite) have been poorly sampled and represent only 2% of Labait xenoliths (Koornneef et al., 2009). This may lead to a sample bias for phlogopite interpretation and hydrous metasomatism.

Alkaline Magmatism During Early Rifting of the East African Rift

Early rifting of the EAR is divided into two branches with opposite rift propagations: rifting in the eastern NTD propagated from north (north and central Kenya, 30–15 Ma) to south (northern Tanzania, <6 Ma; Ebinger et al., 2000; Mana et al., 2015; Furman et al., 2016), whereas rifting in the western part of the Tanzanian Craton propagated from south (Kivu, 8–12 Ma) to north (Toro-Ankole, 0.05 Ma; Ebinger, 1989; Furman, 2007). Both branches have produced highly alkaline, alkaline, and sub-alkaline volcanism along their rift axes (Furman, 2007; Dawson, 2008; Mana et al., 2015; Pouclet et al., 2016). The diversity of erupted lavas in terms of their differentiation (melilitite/basalt to phonolite or trachyte) is linked to fractional crystallization, immiscibility, and assimilation during ascent through the sub-continental lithosphere and continental crust (e.g., Mollel et al., 2009; Dawson, 2012; Mana et al., 2015; Baudouin et al., 2016, 2018), whereas the diversity in terms of magmatic series is related to deep melting processes and the specific mantle sources.

In the NTD, volcanism of different alkalinities occurs along two perpendicular axes (**Figure 1**): the N-S axis erupted highly alkaline magmas such as nephelinite (e.g., Oldoinyo Lengai-Labait; this study; Mana et al., 2012; Mattsson et al., 2013), whereas the W-E axis erupted dominantly alkaline magmas (Essimingor-Kilimanjaro; Nonnotte et al., 2011; Mana et al., 2012, 2015) and sub-alkaline magmas in the western part close to the Tanzanian Craton (i.e., Ngorongoro-Olmoti; Nonnotte, 2007; Mollel et al., 2008, 2009). Although there is a clear correlation between the alkalinity of magmas and their geographical alignment, we found no obvious correlations between eruptive age, alkalinity, depth of partial melting, or mantle source.

Along the N-S axis of the NTD, highly alkaline magmas are the product of very low degrees of partial melting (<1%; this study; Mattsson et al., 2013) of different mantle sources at various depths. From north to south, the depth of partial melting increases and the mantle sources change from (1) CO_2-rich amphibole-lherzolite at shallow depth (∼75–90 km) in the Engaruka-Natron basin (Oldoinyo Lengai; Mattsson et al., 2013), to (2) amphibole-bearing garnet lherzolite at intermediate depth (∼110–140 km at Burko; Mana et al., 2012), and finally to (3) CO_2-rich phlogopite-bearing garnet lherzolite near or below the LAB at 150–160 km depth (Labait; this study; Dawson et al., 1997). The estimated depth of partial melting in the southern part of the NTD is well supported by the presence of deep refractory mantle xenoliths in Labait lavas (>150 km, **Figure 10**; Lee and Rudnick, 1999) and the thick cratonic lithosphere (on-craton eruption; e.g., Dawson et al., 1997; Craig et al., 2011). Alkaline and sub-alkaline magmas erupted along the W-E axis are related to high degrees of partial melting (2–6%) of amphibole-bearing garnet lherzolite at 85–140 km (Nonnotte, 2007; Mana et al., 2015). They erupted at the craton-edge where asthenospheric upwelling may have proceeded to shallow levels, leading to common alkali basalts similar to those observed north of the NTD in central Kenya, which represents a more mature stage of rifting (e.g., Ebinger et al., 2000; Roex et al., 2001).

The relationships between magmatism and rift dynamics observed in the eastern EAR are similar to those observed in the western EAR despite their opposite rift propagations. In the western EAR, magmatism evolved from basalt-basanite at Kivu (south) to K-nephelinite at Toro-Ankole (north) during early stage rifting (Pouclet et al., 1981, 2016; Chakrabarti et al., 2009; Rosenthal et al., 2009) are also associated with peridotite, pyroxenite and glimmerite xenoliths (Muravyeva and Senin, 2018). Alkaline rocks are potassic, attesting to the presence of a potassium-rich mantle source beneath the western part of the Tanzanian Craton (up to 7 wt% K_2O in melt; Pouclet et al., 1981; Rogers et al., 1998). Primary magmas from the north of the western rift originate from the greatest melting depths (>140 km in the presence of phlogopite at Toro-Ankole), and the depth of melting becomes gradually shallower toward the south of the western branch (<90 km in the presence of both amphibole and phlogopite), similar to the observed depth-of-melting in the east branch of EAR (Rosenthal et al., 2009; Foley et al., 2012). The mantle source of potassic magmatism has been characterized as two metasomatic assemblages of phlogopite-clinopyroxenite and a carbonate-rich garnet-free assemblage resulting from kimberlitic-like melt impregnation and crystallization (e.g., Rosenthal et al., 2009; Foley et al., 2012). The asthenospheric source beneath the West branch of EAR is CO_2-rich and highly metasomatized leading to the genesis of ultramafic and potassic primary melt (Foley et al., 2012; Foley and Fischer, 2017).

The low volume of highly alkaline volcanism in both the western and eastern rift branches may be related to the low degrees of partial melting and the deep thermal anomaly beneath the thick cratonic lithosphere (e.g., Ebinger and Sleep, 1998). The occurrence of thin, rifted lithosphere in close proximity to thick cratonic heterogeneous lithosphere may generate melting at shallow depth, likely related to rift propagation and/or the plume-related thermal anomaly. The most likely mechanism for producing sub-cratonic lithospheric heterogeneities is the

accumulation of low-degree partial melts from the convecting depleted asthenospheric mantle (e.g., this study, McKenzie, 1989; Lee and Rudnick, 1999; Vauchez et al., 2005; Baptiste et al., 2015; Chin, 2018).

The variability of the mantle sources of potassic and alkaline volcanism between the western and eastern branches of the EAR may also reflect different sub-cratonic lithospheric lithologies beneath the Paleoproterozoic and Neoproterozoic belts underlying the western and eastern branches, respectively (e.g., Corti et al., 2007; Katumwehe et al., 2015).

CONCLUSION

Volcanoes of the Manyara-Balangida rift, associated with early rifting in the East African Rift (northern Tanzania), have erupted primary nephelinites composed of olivine, clinopyroxene, and up to 4 vol% phlogopite. Trace models of Kwaraha and Labait lavas from a low degree of partial melting (0.2–1%) of a garnet-phlogopite-bearing peridotite with a carbonate-rich component (0.3%), consistent with others northern Tanzania lavas. The presence of garnet-bearing mantle xenoliths and the primary melt compositions indicate that melting occurred at depths $\geq$150 km, below the lithosphere-asthenosphere boundary. The partial melting at the earliest stage rifting is the deepest source reported for East branch of East African Rift. The percolation of deep, CO_2-rich and H_2O-bearing highly alkaline magmas may have produced strong heterogeneities through metasomatism process in the thick sub-continental Tanzanian lithospheric mantle. H_2O-bearing magmas percolation has induced phlogopite crystallization in spinel lherzolite and glimmerite lithology weakening the rheology of the Tanzanian lithosphere. These compositional changes are thus major parameters that have influenced the rift propagation near the craton edge, and should be taken into account to explain tectonic deformation at the surface.

DATA AVAILABILITY STATEMENT

The datasets presented in this study can be found online at https://tel.archives-ouvertes.fr/tel-01563231/.

AUTHOR CONTRIBUTIONS

CB carried out the microprobe, icpms, and FTIR analyses. CB and FP contributed to the interpretations and writing. All authors contributed to the article and approved the submitted version.

FUNDING

This research was financially supported by the ANR project CoLiBrEA CTN°LS 104568 and the HATARI project (Tellus-RIFT INSU).

ACKNOWLEDGMENTS

We thank the reviewers for their suggestions and helpful remarks. This work is a part of CB thesis (Baudouin, 2016). We thank Tanzania COSTECH and the French Embassy for help for Research Permits, and the University of Dar es Salaam for their help during field sampling.

SUPPLEMENTARY MATERIAL

The Supplementary Material for this article can be found online at: https://www.frontiersin.org/articles/10.3389/feart.2020.00277/full#supplementary-material

REFERENCES

Adam, J. (1990). The geochemistry and experimental petrology of Sodic alkaline basalts from Oatlands, Tasmania. *J. Petrol.* 31, 1201–1223. doi: 10.1093/petrology/31.6.1201

Adam, J., and Green, T. (2006). Trace element partitioning between mica- and amphibole-bearing garnet lherzolite and hydrous basanitic melt: 1. Experimental results and the investigation of controls on partitioning behaviour. *Contrib. Mineral. Petrol.* 152, 1–17. doi: 10.1007/s00410-006-0085-4

Albarède, F. (1992). How deep do common basaltic magmas form and differentiate? *J. Geophys. Res. Solid Earth* 97, 10997–11009.

Andersen, T., Elburg, M. A., and Erambert, M. (2014). Extreme peralkalinity in delhayelite-and andremeyerite-bearing nephelinite from Nyiragongo volcano, East African Rift. *Lithos* 206, 164–178. doi: 10.1016/j.lithos.2014.07.025

Aubaud, C., Hauri, E. H., and Hirschmann, M. M. (2004). Hydrogen partition coefficients between nominally anhydrous minerals and basaltic melts. *Geophys. Res. Lett.* 31:L20611.

Aulbach, S., Rudnick, R. L., and McDonough, W. F. (2008). Li-Sr-Nd isotope signatures of the plume and cratonic lithospheric mantle beneath the margin of the rifted Tanzanian craton (Labait). *Contrib. Mineral. Petrol.* 155, 79–92. doi: 10.1007/s00410-007-0226-4

Aulbach, S., Rudnick, R. L., and McDonough, W. F. (2011). Evolution of the lithospheric mantle beneath the East African Rift in Tanzania and its potential signatures in rift magmas. *Geol. Soc. Am. Spec. Pap.* 478, 105–125. doi: 10.1130/2011.2478(06)

Baasner, A., Médard, E., Laporte, D., and Hoffer, G. (2016). Partial melting of garnet lherzolite with water and carbon dioxide at 3 GPa using a new melt extraction technique: implications for intraplate magmatism. *Contrib. Mineral. Petrol.* 171, 1–23.

Bailey, K., Lloyd, F., Kearns, S., Stoppa, F., Eby, N., and Woolley, A. (2005). Melilitite at fort portal, Uganda: another dimension to the carbonate volcanism. *Lithos* 85, 15–25. doi: 10.1016/j.lithos.2005.03.019

Baptiste, V., Tommasi, A., Vauchez, A., Demouchy, S., and Rudnick, R. L. (2015). Deformation, hydration, and anisotropy of the lithospheric mantle in an active rift: constraints from mantle xenoliths from the North Tanzanian Divergence of the East African Rift. *Tectonophysics* 639, 34–55. doi: 10.1016/j.tecto.2014.11.011

Baudouin, C. (2016). *Volcanisme Alcalin Associé À L'initiation de la Rupture Continentale: Rift East Africain, Tanzanie, Bassin de Manyara*. Doctoral dissertation, University of Montpellier, Montpellier.

Baudouin, C., Parat, F., Denis, C. M., and Mangasini, F. (2016). Nephelinite lavas at early stage of rift initiation (Hanang volcano, North Tanzanian Divergence). *Contrib. Mineral. Petrol.* 171, 1–20.

Baudouin, C., Parat, F., and Michel, T. (2018). CO2-rich phonolitic melt and carbonatite immiscibility in early stage of rifting: melt inclusions from Hanang

volcano (Tanzania). *J. Volcanol. Geother. Res.* 358, 261–272. doi: 10.1016/j.jvolgeores.2018.05.019

Behrens, H., Romano, C., Nowak, M., Holtz, F., and Dingwell, D. B. (1996). Near-infrared spectroscopic determination of water species in glasses of the system MAlSi3O8 (M = Li, Na, K): an interlaboratory study. *Chem. Geol.* 128, 41–63. doi: 10.1016/0009-2541(95)00162-x

Berndt, J., Koepke, J., and Holtz, F. (2005). An experimental investigation of the influence of water and oxygen fugacity on differentiation of MORB at 200 MPa. *J. Petrol.* 46, 135–167. doi: 10.1093/petrology/egh066

Brey, G. (1978). Origin of olivine melilitites–chemical and experimental constraints. *J. Volcanol. Geother. Res.* 3, 61–88. doi: 10.1016/0377-0273(78)90004-5

Brooker, R. A., Kohn, S. C., Holloway, J. R., and McMillan, P. F. (2001). Structural controls on the solubility of CO2 in silicate melts: part II: IR characteristics of carbonate groups in silicate glasses. *Chem. Geol.* 174, 241–254. doi: 10.1016/s0009-2541(00)00318-1

Carignan, J., Hild, P., Mevelle, G., Morel, J., and Yeghicheyan, D. (2001). Routine analyses of trace elements in geological samples using flow injection and low pressure on-line liquid chromatography coupled to ICP-MS: a study of geochemical reference materials BR, DR-N, UB-N, AN-G and GH. *Geostand. Newsl.* 25, 187–198. doi: 10.1111/j.1751-908x.2001.tb00595.x

Carmichael, I. S., and Ghiorso, M. S. (1990). The effect of oxygen fugacity on the redox state of natural liquids and their crystallizing phases. *Rev. Mineral. Geochem.* 24, 191–212. doi: 10.1515/9781501508769-011

Chakrabarti, R., Basu, A. R., Santo, A. P., Tedesco, D., and Vaselli, O. (2009). Isotopic and geochemical evidence for a heterogeneous mantle plume origin of the Virunga volcanics, Western rift, East African Rift system. *Chem. Geol.* 259, 273–289. doi: 10.1016/j.chemgeo.2008.11.010

Chin, E. J. (2018). Deep crustal cumulates reflect patterns of continental rift volcanism beneath Tanzania. *Contrib. Mineral. Petrol.* 173:85.

Condamine, P., and Médard, E. (2014). Experimental melting of phlogopite-bearing mantle at 1 GPa: implications for potassic magmatism. *Earth Planet. Sci. Lett.* 397, 80–92. doi: 10.1016/j.epsl.2014.04.027

Condamine, P., Médard, E., and Devidal, J. L. (2016). Experimental melting of phlogopite-peridotite in the garnet stability field. *Contrib. Mineral. Petrol.* 171:95.

Corti, G., van Wijk, J., Cloetingh, S., and Morley, C. K. (2007). Tectonic inheritance and continental rift architecture: numerical and analogue models of the East African Rift system. *Tectonics* 26:TC6006.

Craig, T. J., Jackson, J. A., Priestley, K., and McKenzie, D. (2011). Earthquake distribution patterns in Africa: their relationship to variations in lithospheric and geological structure, and their rheological implications. *Geophys. J. Int.* 185, 403–434. doi: 10.1111/j.1365-246x.2011.04950.x

Dasgupta, R., Hirschmann, M. M., and Smith, N. D. (2007). Partial melting experiments of peridotite + CO2 at 3 GPa and genesis of alkalic ocean island basalts. *J. Petrol.* 48, 2093–2124. doi: 10.1093/petrology/egm053

Dasgupta, R., Mallik, A., Tsuno, K., Withers, A. C., Hirth, G., and Hirschmann, M. M. (2013). Carbon-dioxide-rich silicate melt in the Earth's upper mantle. *Nature* 493, 211–215. doi: 10.1038/nature11731

Dawson, J. B. (2008). *The Gregory Rift Valley and Neogene-Recent Volcanoes of Northern Tanzania*. London: Geological Society of London.

Dawson, J. B. (2012). Nephelinite–melilitite–carbonatite relationships: evidence from pleistocene–recent volcanism in northern Tanzania. *Lithos* 152, 3–10. doi: 10.1016/j.lithos.2012.01.008

Dawson, J. B., James, D., Paslick, C., and Halliday, A. M. (1997). Ultrabasic potassic low-volume magmatism and continental rifting in north-central Tanzania: association with enhanced heat flow. *Russ. Geol. Geophys.* 38, 69–81.

Dawson, J. B., Powell, D. G., and Reid, A. M. (1970). Ultrabasic xenoliths and lava from the Lashaine volcano, northern Tanzania. *J. Petrol.* 11, 519–548. doi: 10.1093/petrology/11.3.519

Dawson, J. B., and Smith, J. V. (1977). The MARID (mica-amphibole-rutile-ilmenite-diopside) suite of xenoliths in kimberlite. *Geochim. Cosmochim. Acta* 41, 309–323. doi: 10.1016/0016-7037(77)90239-3

Dawson, J. B., and Smith, J. V. (1988). Metasomatised and veined upper-mantle xenoliths from Pello Hill, Tanzania: evidence for anomalously-light mantle beneath the Tanzanian sector of the East African Rift Valley. *Contrib. Mineral. Petrol.* 100, 510–527. doi: 10.1007/bf00371380

Dawson, J. B., and Smith, J. V. (1992). Olivine-mica pyroxenite xenoliths from northern Tanzania: metasomatic products of upper-mantle peridotite. *J. Volcanol. Geother. Res.* 50, 131–142. doi: 10.1016/0377-0273(92)90041-b

Demouchy, S., and Bolfan-Casanova, N. (2016). Distribution and transport of hydrogen in the Lithospheric mantle: a review. *Lithos* 240, 402–425. doi: 10.1016/j.lithos.2015.11.012

Denis, C. M., Alard, O., and Demouchy, S. (2015). Water content and hydrogen behaviour during metasomatism in the uppermost mantle beneath Ray Pic volcano (Massif Central, France). *Lithos* 236, 256–274. doi: 10.1016/j.lithos.2015.08.013

Ebinger, C. J. (1989). Tectonic development of the western branch of the East-African rift system. *Geol. Soc. Am. Bull.* 101, 885–903. doi: 10.1130/0016-7606(1989)101<0885:tdotwb>2.3.co;2

Ebinger, C. J., and Sleep, N. H. (1998). Cenozoic magmatism throughout east Africa resulting from impact of a single plume. *Nature* 395, 788–791. doi: 10.1038/27417

Ebinger, C. J., Yemane, T., Harding, D. J., Tesfaye, S., Kelley, S., and Rex, D. C. (2000). Rift deflection, migration, and propagation: linkage of the Ethiopian and Eastern rifts, Africa. *Geol. Soc. Am. Bull.* 112, 163–176. doi: 10.1130/0016-7606(2000)112<163:rdmapl>2.0.co;2

Eccles, D. R., Heaman, L. M., Luth, R. W., and Creaser, R. A. (2004). Petrogenesis of the late cretaceous northern Alberta kimberlite province. *Lithos* 76, 435–459. doi: 10.1016/j.lithos.2004.03.046

Eggler, D. H., and Holloway, J. R. (1977). Partial melting of peridotite in the presence of H2O and CO2: principles and review. *Magma Genesis* 96, 15–36.

Etame, J., Suh, C. E., Gerard, M., and Bilong, P. (2012). Phillipsite formation in nephelinitic rocks in response to hydrothermal alteration at Mount Etinde, Cameroon. *Geochemistry* 72, 31–37. doi: 10.1016/j.chemer.2011.08.002

Foley, S. F. (1993). An experimental study of olivine lamproite: first results from the diamond stability field. *Geochim. Cosmochim. Acta* 57, 483–489. doi: 10.1016/0016-7037(93)90448-6

Foley, S. F., and Fischer, T. P. (2017). An essential role for continental rifts and lithosphere in the deep carbon cycle. *Nat. Geosci.* 10, 897–902. doi: 10.1038/s41561-017-0002-7

Foley, S. F., Link, K., Tiberindwa, J. V., and Barifaijo, E. (2012). Patterns and origin of igneous activity around the Tanzanian craton. *J. Afr. Earth Sci.* 62, 1–18. doi: 10.1016/j.jafrearsci.2011.10.001

Foley, S. F., Yaxley, G. M., Rosenthal, A., Buhre, S., Kiseeva, E. S., Rapp, R. P., et al. (2009). The composition of near-solidus melts of peridotite in the presence of CO2 and H2O between 40 and 60 kbar. *Lithos* 112, 274–283. doi: 10.1016/j.lithos.2009.03.020

Förster, M. W., Preleviæ, D., Schmück, H. R., Buhre, S., Marschall, H. R., Mertz-Kraus, R., et al. (2018). Melting phlogopite-rich MARID: lamproites and the role of alkalis in olivine-liquid Ni-partitioning. *Chem. Geol.* 476, 429–440. doi: 10.1016/j.chemgeo.2017.11.039

Frey, F. A., Green, D. H., and Roy, S. D. (1978). Integrated models of basalt petrogenesis: a study of quartz tholeiites to olivine melilitites from south eastern Australia utilizing geochemical and experimental petrological data. *J. Petrol.* 19, 463–513. doi: 10.1093/petrology/19.3.463

Fujimaki, H., Tatsumoto, M., and Aoki, K. I. (1984). Partition coefficients of Hf, Zr, and REE between phenocrysts and groundmasses. *J. Geophys. Res. Solid Earth* 89, B662–B672.

Furman, T. (2007). Geochemistry of East African Rift basalts: an overview. *J. Afr. Earth Sci.* 48, 147–160. doi: 10.1016/j.jafrearsci.2006.06.009

Furman, T., Nelson, W. R., and Elkins-Tanton, L. T. (2016). Evolution of the East African rift: drip magmatism, lithospheric thinning and mafic volcanism. *Geochim. Cosmochim. Acta* 185, 418–434. doi: 10.1016/j.gca.2016.03.024

Gardès, E., Laumonier, M., Massuyeau, M., and Gaillard, F. (2020). Unravelling partial melt distribution in the oceanic low velocity zone. *Earth Planet. Sci. Lett.* 540:116242. doi: 10.1016/j.epsl.2020.116242

Gibson, S. A., McMahon, S. C., Day, J. A., and Dawson, J. B. (2013). Highly refractory lithospheric mantle beneath the Tanzanian craton: evidence from Lashaine pre-metasomatic garnet-bearing peridotites. *J. Petrol.* 54, 1503–1546. doi: 10.1093/petrology/egt020

Green, D. H., and Falloon, T. J. (1998). "Pyrolite: a Ringwood concept and its current expression," in *The Earth's Mantle: Composition, Structure, and Evolution*, ed. I. Jackson, (Cambridge: Cambridge University Press), 311–378. doi: 10.1017/cbo9780511573101.010

Green, D. H., and Falloon, T. J. (2015). Mantle-derived magmas: intraplate, hotspots and mid-ocean ridges. *Sci. Bull.* 60, 1873–1900. doi: 10.1007/s11434-015-0920-y

Green, D. H., Hibberson, W. O., Rosenthal, A., Kovács, I., Yaxley, G. M., Falloon, T. J., et al. (2014). Experimental study of the influence of water on melting and phase assemblages in the upper mantle. *J. Petrol.* 55, 2067–2096. doi: 10.1093/petrology/egu050

Grégoire, M., Bell, D., and Le Roex, A. (2002). Trace element geochemistry of phlogopite-rich mafic mantle xenoliths: their classification and their relationship to phlogopite-bearing peridotites and kimberlites revisited. *Contrib. Mineral. Petrol.* 142, 603–625. doi: 10.1007/s00410-001-0315-8

Griffin, W. L., Powell, W. J., Pearson, N. J., and O'Reilly, S. Y. (2008). GLITTER: data reduction software for laser ablation ICP-MS. Laser Ablation-ICP-MS in the earth sciences. *Mineral. Assoc. Canada Short Course Ser.* 40, 204–207.

Gudfinnsson, G. H., and Presnall, D. C. (2005). Continuous gradations among primary carbonatitic, kimberlitic, melilititic, basaltic, picritic, and komatiitic melts in equilibrium with garnet lherzolite at 3–8 GPa. *J. Petrol.* 46, 1645–1659. doi: 10.1093/petrology/egi029

Hammouda, T., and Keshav, S. (2015). Melting in the mantle in the presence of carbon: review of experiments and discussion on the origin of carbonatites. *Chem. Geol.* 418, 171–188.

Hauri, E. H., Gaetani, G. A., and Green, T. H. (2006). Partitioning of water during melting of the Earth's upper mantle at H2O-undersaturated conditions. *Earth Planet. Sci. Lett.* 248, 715–734. doi: 10.1016/j.epsl.2006.06.014

Hofmann, A. W. (1988). Chemical differentiation of the Earth: the relationship between mantle, continental crust, and oceanic crust. *Earth Planet. Sci. Lett.* 90, 297–314. doi: 10.1016/0012-821x(88)90132-x

Hudgins, T. R., Mukasa, S. B., Simon, A. C., Moore, G., and Barifaijo, E. (2015). Melt inclusion evidence for CO2-rich melts beneath the western branch of the East African Rift: implications for long-term storage of volatiles in the deep lithospheric mantle. *Contrib. Mineral. Petrol.* 169:46.

Hui, H., Peslier, A. H., Rudnick, R. L., Simonetti, A., and Neal, C. R. (2015). Plume-cratonic lithosphere interaction recorded by water and other trace elements in peridotite xenoliths from the Labait volcano, Tanzania. *Geochem. Geophys. Geosyst.* 16, 1687–1710. doi: 10.1002/2015gc005779

Huppert, H. E., and Sparks, R. S. J. (1985). Cooling and contamination of mafic and ultramafic magmas during ascent through continental crust. *Earth Planet. Sci. Lett.* 74, 371–386. doi: 10.1016/s0012-821x(85)80009-1

Ivanikov, V. V., Rukhlov, A. S., and Bell, K. (1998). Magmatic evolution of the melilitite–carbonatite–nephelinite dyke series of the Turiy Peninsula (Kandalaksha Bay, White Sea, Russia). *J. Petrol.* 39, 2043–2059. doi: 10.1093/petroj/39.11-12.2043

Johnson, L. H., Jones, A. P., Church, A. A., and Taylor, W. R. (1997). Ultramafic xenoliths and megacrysts from a melilitite tuff cone, Deeti, northern Tanzania. *J. Afr. Earth Sci.* 25, 29–42. doi: 10.1016/s0899-5362(97)00060-2

Jones, A. P., Smith, J. V., and Dawson, J. B. (1982). Mantle metasomatism in 14 veined peridotites from Bultfontein Mine, South Africa. *J. Geol.* 90, 435–453. doi: 10.1086/628695

Jones, A. P., Smith, J. V., and Dawson, J. B. (1983). Glasses in mantle xenoliths from Olmani, Tanzania. *J. Geol.* 91, 167–178. doi: 10.1086/628754

Katumwehe, A. B., Abdelsalam, M. G., and Atekwana, E. A. (2015). The role of pre-existing Precambrian structures in rift evolution: the Albertine and Rhino grabens, Uganda. *Tectonophysics* 646, 117–129. doi: 10.1016/j.tecto.2015.01.022

Keller, J., Zaitsev, A. N., and Wiedenmann, D. (2006). Primary magmas at Oldoinyo Lengai: the role of olivine melilitites. *Lithos* 91, 150–172. doi: 10.1016/j.lithos.2006.03.014

Keller, T., and Katz, R. F. (2016). The role of volatiles in reactive melt transport in the asthenosphere. *J. Petrol.* 57, 1073–1108. doi: 10.1093/petrology/egw030

Klaudius, J., and Keller, J. (2006). Peralkaline silicate lavas at Oldoinyo Lengai, Tanzania. *Lithos* 91, 173–190. doi: 10.1016/j.lithos.2006.03.017

Koornneef, J. M., Davies, G. R., Döpp, S. P., Vukmanovic, Z., Nikogosian, I. K., and Mason, P. R. (2009). Nature and timing of multiple metasomatic events in the sub-cratonic lithosphere beneath Labait, Tanzania. *Lithos* 112, 896–912. doi: 10.1016/j.lithos.2009.04.039

Konzett, J., and Ulmer, P. (1999). The stability of hydrous potassic phases in lherzolitic mantle—an experimental study to 9.5 GPa in simplified and natural bulk compositions. *J. Petrol.* 40, 629–652. doi: 10.1093/petroj/40.4.629

Kramers, J. D., Roddick, J. C. M., and Dawson, J. B. (1983). Trace element and isotope studies on veined, metasomatic and "MARID" xenoliths from Bultfontein, South Africa. *Earth Planet. Sci. Lett.* 65, 90–106. doi: 10.1016/0012-821x(83)90192-9

Kushiro, I. (1969). Clinopyroxene solid solutions formed by reactions between diopside and plagioclase at high pressures. *Mineral. Soc. Amer. Spec. Pap.* 2, 179–191.

Le Bas, M. J. (1989). Nephelinitic and basanitic rocks. *J. Petrol.* 30, 1299–1312. doi: 10.1093/petrology/30.5.1299

Le Gall, B., Nonnotte, P., Rolet, J., Benoit, M., Guillou, H., Mousseau-Nonnotte, M., et al. (2008). Rift propagation at craton margin: distribution of faulting and volcanism in the North Tanzanian Divergence (East Africa) during Neogene times. *Tectonophysics* 448, 1–19.

Lee, C. T., and Rudnick, R. L. (1999). "Compositionally stratified cratonic lithosphere: petrology and geochemistry of peridotite xenoliths from the Labait volcano, Tanzania," in *Proceedings of the VIIth International Kimberlite Conference*, Vol. 1, Cape Town, 503–521.

Lee, W. J., Huang, W. L., and Wyllie, P. (2000). Melts in the mantle modeled in the system CaO–MgO–SiO2–CO2 at 2.7 GPa. *Contrib. Mineral. Petrol.* 138, 199–213. doi: 10.1007/s004100050557

Luth, R. W. (1997). Experimental study of the system phlogopite-diopside from 3.5 to 17 GPa. *Am. Min.* 82, 1198–1209. doi: 10.2138/am-1997-11-1216

Lloyd, F. E., Woolley, A. R., Stoppa, F., and Eby, G. N. (2002). Phlogopite-biotite parageneses from the K-mafic-carbonatite effusive magmatic association of Katwe-Kikorongo, SW Uganda. *Mineral. Petrol.* 74, 299–322. doi: 10.1007/s007100200008

Maaløe, S., James, D., Smedley, P., Petersen, S., and Garmann, L. B. (1992). The Koloa volcanic suite of Kauai, Hawaii. *J. Petrol.* 33, 761–784. doi: 10.1093/petrology/33.4.761

MacDonald, R., Rogers, N. W., Fitton, J. G., Black, S., and Smith, M. (2001). Plume–lithosphere interactions in the generation of the basalts of the Kenya Rift, East Africa. *J. Petrol.* 42, 877–900. doi: 10.1093/petrology/42.5.877

Mana, S., Furman, T., Carr, M. J., Mollel, G. F., Mortlock, R. A., Feigenson, M. D., et al. (2012). Geochronology and geochemistry of the Essimingor volcano: melting of metasomatized lithospheric mantle beneath the North Tanzanian Divergence zone (East African Rift). *Lithos* 155, 310–325. doi: 10.1016/j.lithos.2012.09.009

Mana, S., Furman, T., Turrin, B. D., Feigenson, M. D., and Swisher, C. C. (2015). Magmatic activity across the East African North Tanzanian Divergence Zone. *J. Geol. Soc.* 172, 368–389. doi: 10.1144/jgs2014-072

Masotta, M., Mollo, S., Freda, C., Gaeta, M., and Moore, G. (2013). Clinopyroxene–liquid thermometers and barometers specific to alkaline differentiated magmas. *Contrib. Mineral. Petrol.* 166, 1545–1561. doi: 10.1007/s00410-013-0927-9

Mattsson, H. B., Nandedkar, R. H., and Ulmer, P. (2013). Petrogenesis of the melilititic and nephelinitic rock suites in the Lake Natron–Engaruka monogenetic volcanic field, northern Tanzania. *Lithos* 179, 175–192. doi: 10.1016/j.lithos.2013.07.012

Maumus, J., Laporte, D., and Schiano, P. (2004). Dihedral angle measurements and infiltration property of SiO2-rich melts in mantle peridotite assemblages. *Contrib. Mineral. Petrol.* 148, 1–12. doi: 10.1007/s00410-004-0595-x

McKenzie, D. (1989). Some remarks on the movement of small melt fractions in the mantle. *Earth Planet. Sci. Lett.* 95, 53–72. doi: 10.1016/0012-821x(89)90167-2

McKenzie, D., and O'Nions, R. K. (1991). Partial melt distributions from inversion of rare earth element concentrations. *J. Petrol.* 32, 1021–1091. doi: 10.1093/petrology/32.5.1021

Métrich, N., and Wallace, P. J. (2008). Volatile abundances in basaltic magmas and their degassing paths tracked by melt inclusions. *Rev. Mineral. Geochem.* 69, 363–402. doi: 10.1515/9781501508486-011

Mollel, G. F., Swisher, C. C., Feigenson, M. D., and Carr, M. J. (2008). Geochemical evolution of Ngorongoro Caldera, Northern Tanzania: implications for crust–magma interaction. *Earth Planet. Sci. Lett.* 271, 337–347. doi: 10.1016/j.epsl.2008.04.014

Mollel, G. F., Swisher, C. C., McHenry, L. J., Feigenson, M. D., and Carr, M. J. (2009). Petrogenesis of basalt–trachyte lavas from Olmoti Crater, Tanzania. *J. Afr. Earth Sci.* 54, 127–143. doi: 10.1016/j.jafrearsci.2009.03.008

Mourão, C., Mata, J., Doucelance, R., Madeira, J., Millet, M. A., and Moreira, M. (2012). Geochemical temporal evolution of Brava Island magmatism: constraints on the variability of Cape Verde mantle sources and on carbonatite–silicate magma link. *Chem. Geol.* 334, 44–61. doi: 10.1016/j.chemgeo.2012.09.031

Moussallam, Y., Morizet, Y., Massuyeau, M., Laumonier, M., and Gaillard, F. (2015). CO2 solubility in kimberlite melts. *Chem. Geol.* 418, 198–205. doi: 10.1016/j.chemgeo.2014.11.017

Muravyeva, N. S., and Senin, V. G. (2018). Xenoliths from Bunyaruguru volcanic field: some insights into lithology of East African Rift upper mantle. *Lithos* 296, 17–36. doi: 10.1016/j.lithos.2017.10.023

Neukirchen, F., Finkenbein, T., and Keller, J. (2010). The Lava sequence of the East African Rift escarpment in the Oldoinyo Lengai–Lake Natron sector, Tanzania. *J. Afr. Earth Sci.* 58, 734–751. doi: 10.1016/j.jafrearsci.2010.06.002

Nonnotte, P. (2007). *Etude Volcano-Tectonique de la Zone de Divergence Nord Tanzanienne (Terminaison Sud du Rift Kenyan). Caractérisation Pétrologique et Géochimique du Volcanisme Récent (8 Ma–Actuel) et du Manteau Source. Contraintes de Mise en Place*. Doctoral dissertation, Université de Bretagne occidentale, Brest.

Nonnotte, P., Benoit, M., Le Gall, B., Hémond, C., Rolet, J., Cotten, J., et al. (2011). Petrology and geochemistry of alkaline lava series, Kilimanjaro, Tanzania: new constraints on petrogenetic processes. *Geol. Soc. Am. Spec. Pap.* 478, 127–158. doi: 10.1130/2011.2478(07)

Novella, D., Bolfan-Casanova, N., Nestola, F., and Harris, J. W. (2015). H2O in olivine and garnet inclusions still trapped in diamonds from the Siberian craton: implications for the water content of cratonic lithosphere peridotites. *Lithos* 230, 180–183. doi: 10.1016/j.lithos.2015.05.013

Oppenheimer, C., Pyle, D. M., and Barclay, J. (2003). *Volcanic Degassing*. London: Geological Society of London.

Parat, F., Holtz, F., René, M., and Almeev, R. (2010). Experimental constraints on ultrapotassic magmatism from the Bohemian Massif (durbachite series, Czech Republic). *Contrib. Mineral. Petrol.* 159, 331–347. doi: 10.1007/s00410-009-0430-5

Paslick, C. R., Halliday, A. N., Lange, R. A., James, D., and Dawson, J. B. (1996). Indirect crustal contamination: evidence from isotopic and chemical disequilibria in minerals from alkali basalts and nephelinites from northern Tanzania. *Contrib. Mineral. Petrol.* 125, 277–292. doi: 10.1007/s004100050222

Paterson, M. S. (1982). The determination of hydroxyl by infrared absorption in quartz, silicate glasses, and similar materials. *Bull. Soc. Fr. Minéral. Crist.* 105, 20–29. doi: 10.3406/bulmi.1982.7582

Platz, T., Foley, S. F., and André, L. (2004). Low-pressure fractionation of the Nyiragongo volcanic rocks, Virunga Province, D.R. Congo. *J. Volcanol. Geother. Res.* 136, 269–295. doi: 10.1016/j.jvolgeores.2004.05.020

Pouclet, A., Bellon, H., and Bram, K. (2016). The Cenozoic volcanism in the Kivu rift: assessment of the tectonic setting, geochemistry, and geochronology of the volcanic activity in the South-Kivu and Virunga regions. *J. Afr. Earth Sci.* 121, 219–246. doi: 10.1016/j.jafrearsci.2016.05.026

Pouclet, A., Menot, R. P., and Piboule, M. (1981). Discriminant factor-analysis applied to central Africa rift lavas (Zaire, Rwanda, Uganda). *C. R. Acad. Sci. II* 292:679.

Putirka, K. D. (2008). Thermometers and barometers for volcanic systems. *Rev. Mineral. Geochem.* 69, 61–120. doi: 10.1515/9781501508486-004

Roex, A. P., Späth, A., and Zartman, R. E. (2001). Lithospheric thickness beneath the southern Kenya Rift: implications from basalt geochemistry. *Contrib. Mineral. Petrol.* 142, 89–106. doi: 10.1007/s004100100273

Rogers, N. W., Hawkesworth, C. J., and Palacz, Z. A. (1992). Phlogopite in the generation of olivine-melilitites from Namaqualand, South Africa and implications for element fractionation processes in the upper mantle. *Lithos* 28, 347–365. doi: 10.1016/0024-4937(92)90014-p

Rogers, N. W., James, D., Kelley, S. P., and De Mulder, M. (1998). The generation of potassic lavas from the eastern Virunga province, Rwanda. *J. Petrol.* 39, 1223–1247. doi: 10.1093/petroj/39.6.1223

Rosenthal, A., Foley, S. F., Pearson, D. G., Nowell, G. M., and Tappe, S. (2009). Petrogenesis of strongly alkaline primitive volcanic rocks at the propagating tip of the western branch of the East African Rift. *Earth Planet. Sci. Lett.* 284, 236–248. doi: 10.1016/j.epsl.2009.04.036

Rudnick, R. L., Ireland, T. R., Gehrels, G., Irving, A. J., Chesley, J. T., and Hanchar, J. M. (1999). "Dating mantle metasomatism: U–Pb geochronology of zircons in cratonic mantle xenoliths from Montana and Tanzania," in *Proceedings of the 7th International Kimberlite Conference*, Vol. 2, Cape Town, 728–735.

Rudnick, R. L., McDonough, W. F., and Chappell, B. W. (1993). Carbonatite metasomatism in the northern Tanzanian mantle: petrographic and geochemical characteristics. *Earth Planet. Sci. Lett.* 114, 463–475. doi: 10.1016/0012-821x(93)90076-l

Sato, K., Katsura, T., and Ito, E. (1997). Phase relations of natural phlogopite with and without enstatite up to 8 GPa: implication for mantle metasomatism. *Earth Planet. Sci. Lett.* 146, 511–526. doi: 10.1016/s0012-821x(96)00246-4

Schmidt, K. H., Bottazzi, P., Vannucci, R., and Mengel, K. (1999). Trace element partitioning between phlogopite, clinopyroxene and leucite lamproite melt. *Earth Planet. Sci. Lett.* 168, 287–299. doi: 10.1016/s0012-821x(99)00056-4

Selway, K., Yi, J., Karato, S. I. (2014). Water content of the Tanzanian lithosphere from magnetotelluric data: implications for cratonic growth and stability. *Earth Planet. Sci. Lett.* 388, 175–186. doi: 10.1016/j.epsl.2013.11.024

Simonetti, A., Shore, M., and Bell, K. (1996). Diopside phenocrysts from nephelinite lavas, Napak Volcano, eastern Uganda; evidence for magma mixing. *Can. Mineral.* 34, 411–421.

Soltanmohammadi, A., Gregoire, M., Rabinowicz, M., Gerbault, M., Ceuleneer, G., Rahgoshay, M., et al. (2018). Transport of volatile-rich melt from the mantle transition zone via compaction pockets: implications for mantle metasomatism and the origin of alkaline lavas in the Turkish–Iranian plateau. *J. Petrol.* 59, 2273–2310. doi: 10.1093/petrology/egy097

Stagno, V., Ojwang, D. O., McCammon, C. A., and Frost, D. J. (2013). The oxidation state of the mantle and the extraction of carbon from Earth's interior. *Nature.* 493, 84–88. doi: 10.1038/nature11679

Streck, M. J., Leeman, W. P., and Chesley, J. (2007). High-magnesian andesite from Mount Shasta: a product of magma mixing and contamination, not a primitive mantle melt. *Geology* 35, 351–354.

Sun, S. S., and McDonough, W. S. (1989). Chemical and isotopic systematics of oceanic basalts: implications for mantle composition and processes. *Geol. Soc. Lond. Spec. Publ.* 42, 313–345. doi: 10.1144/gsl.sp.1989.042.01.19

Toplis, M. J., and Carroll, M. R. (1995). An experimental study of the influence of oxygen fugacity on Fe-Ti oxide stability, phase relations, and mineral—melt equilibria in ferro-basaltic systems. *J. Petrol.* 36, 1137–1170. doi: 10.1093/petrology/36.5.1137

Trønnes, R. G. (2002). Stability range and decomposition of potassic richterite and phlogopite end members at 5–15 GPa. *Mineral. Petrol.* 74, 129–148. doi: 10.1007/s007100200001

Vauchez, A., Dineur, F., and Rudnick, R. (2005). Microstructure, texture and seismic anisotropy of the lithospheric mantle above a mantle plume: insights from the Labait volcano xenoliths (Tanzania). *Earth Planet. Sci. Lett.* 232, 295–314. doi: 10.1016/j.epsl.2005.01.024

Waters, F. G. (1987). A suggested origin of MARID xenoliths in kimberlites by high pressure crystallization of an ultrapotassic rock such as lamproite. *Contrib. Mineral. Petrol.* 95, 523–533. doi: 10.1007/bf00402210

Woolley, A. R., and Kjarsgaard, B. A. (2008). Paragenetic types of carbonatite as indicated by the diversity and relative abundances of associated silicate rocks: evidence from a global database. *Can. Mineral.* 46, 741–752. doi: 10.3749/canmin.46.4.741

Yoder, H. S., and Kushiro, I. (1969). Melting of a hydrous phase: phlogopite. *Am. J. Sci.* 267, 558–582.

Zaitsev, A. N., Marks, M. A. W., Wenzel, T., Spratt, J., Sharygin, V. V., Strekopytov, S., et al. (2012). Mineralogy, geochemistry and petrology of the phonolitic to nephelinitic Sadiman volcano, Crater Highlands, Tanzania. *Lithos* 152, 66–83. doi: 10.1016/j.lithos.2012.03.001

Conflict of Interest: The authors declare that the research was conducted in the absence of any commercial or financial relationships that could be construed as a potential conflict of interest.